Effects of oxygen on the magnetic order of the rare-earth ions in $RBa_2Cu_3O_{6+x}$ (R = Dy, Er, Nd)

T. W. Clinton and J. W. Lynn
Center for Superconductivity Research, Department of Physics, University of Maryland, College Park, Maryland 20742 and National Institute of Standards and Technology, Reactor Radiation Division, Gaithersburg, Maryland 20899

J. Z. Liu, Y. X. Jia, T. J. Goodwin, and R. N. Shelton
Department of Physics, University of California, Davis, California 95616

B. W. Lee, M. Buchgeister, and M. B. Maple
Department of Physics and Institute for Pure and Applied Physical Sciences, University of California at San Diego, La Jolla, California 92093

J. L. Peng
Center for Superconductivity Research, Department of Physics, University of Maryland, College Park, Maryland 20742
(Received 25 August 1993; revised manuscript received 23 January 1995)

Neutron diffraction has been used to study the effects of oxygen on the magnetic order of the rare-earth ions in $RBa_2Cu_3O_{6+x}$ (R=Dy, Er, Nd). For fully oxygenated superconducting (T_c=92 K) $ErBa_2Cu_3O_7$, two-dimensional (2D) short-range magnetic correlations are observed just above the ordering temperature T_N=0.62 K, while at T_N long-range correlations develop in the a-b plane, inducing 3D long-range order. Below T_N the sublattice magnetization is found to obey Onsager's exact solution of the 2D $S=\frac{1}{2}$ Ising model. For oxygen-reduced ($x\approx 0.6$) superconducting $ErBa_2Cu_3O_{6.6}$ the 3D ordering temperature is lowered to $T_N\simeq 0.48$ K. For insulating $ErBa_2Cu_3O_{6+x}$ ($x\approx 0$) *neither* 2D nor 3D long-range order develops, as *only* 2D short-range correlations are observed. For $DyBa_2Cu_3O_7$ ($T_c\simeq 92$ K) 3D long-range order occurs at $T_N\simeq 0.93$ K, with spins coupled antiferromagnetically along all three crystallographic axes. As we reduce the oxygen concentration the 3D magnetic ordering temperature decreases. In addition, for a concentration $0.54\leq x_c<1$, still in the superconducting phase, the spin configuration changes along the c-axis to ferromagnetic. In the insulating phase, $x\lesssim 0.4$, we observe *both* 2D and 3D diffuse scattering developing below 2 K, but 3D long-range order never occurs. In our highest oxygenated $NdBa_2Cu_3O_{6.94}$ ($T_c\simeq 92$ K), 3D long-range order develops below $T_N\simeq 0.53$ K. For a small reduction of oxygen to $x=0.78$, we observe drastic effects on the Nd order as *only* short-range 2D correlations are found at low temperatures. At nonsuperconducting $x=0.45$, 3D correlations develop at low temperatures, yet long-range order still does not occur. For $x=0.3$, 3D long-range order is reestablished, developing below $T_N\simeq 1.5$ K, three times that of the fully oxygenated material. Though the oxygen dependence of the rare-earth magnetism varies between the three compounds we have studied, our results indicate there is significant coupling between the chain layer oxygen and the rare-earth ions in each case.

I. INTRODUCTION

The rare-earth magnetic interactions in the R123 systems have generally been considered to be rather simple. This notion was motivated partly by early experiments which showed that substitution of other rare earths for yttrium in $YBa_2Cu_3O_7$ did not affect superconductivity, suggesting that the rare-earth sublattice is electronically isolated from the superconducting Cu-O planes.[1] In addition, the ordering temperatures for the magnetic rare earths are near 1 K, which for the heavy rare earths is in the range where magnetic dipole-dipole interactions are important, and this also suggests that the rare-earth ions are isolated. This picture is consistent with measurements which found no difference in the magnetic order of Gd in fully deoxygenated $GdBa_2Cu_3O_6$ as compared to fully oxygenated $GdBa_2Cu_3O_7$.[11] However, more recent specific-heat and neutron-scattering measurements on the oxygen dependence of the magnetic order of Er,[2,3] Dy,[3,4] and Nd (Refs. 3 and 5) have indicated that chain layer oxygen vacancies affects the rare-earth magnetic order.

We will show in this work that indeed oxygen has a strong influence on the magnetic order of rare-earth ions. In going from fully oxygenated superconducting $ErBa_2Cu_3O_7$ to nominally oxygenated insulating $ErBa_2Cu_3O_{6+x}$ ($x\approx 0$) we go from a rare-earth system that exhibits three-dimensional (3D) long-range order at low temperature to a system with only 2D short-range magnetic correlations at the lowest achievable temperatures (T=60 mK). We have made measurements on single crystals with three different oxygen concentrations: fully oxygenated $x\simeq 1$, partially deoxygenated $x\approx 0.6$, and nominally oxygenated $x\approx 0$.

In addition, we have made measurements on several single crystals as well as powder samples of $DyBa_2Cu_3O_{6+x}$ over the full range of oxygen concentra-

 ©1995 The American Physical Society

tions $0 \lesssim x \lesssim 1$. For fully oxygenated, superconducting $DyBa_2Cu_3O_7$ we observe the 2D and 3D magnetic nature of the Dy order, analogous to the magnetic behavior of Er observed in $ErBa_2Cu_3O_7$.[6] Long-range order develops at $T_N \simeq 0.93$ K with Dy spins coupled antiferromagnetically along all three crystallographic axes, while above T_N we observe a rod of scattering, characteristic of 2D behavior. As the oxygen concentration is reduced the ordering temperature decreases, and at an oxygen concentration still in the superconducting phase the spin configuration changes along the c axis to ferromagnetic. For $x \approx 0$, where the Cu spins also exhibit long-range antiferromagnetic order, the magnetic behavior is drastically altered. Quite unexpectedly, *both* 2D and 3D magnetic correlations develop below ≈ 2 K, but 3D long-range order never develops even though the 2D correlations become long range within our experimental resolution.

Finally, we report our results from neutron-scattering and specific-heat measurements on the oxygen dependence of the magnetic order of Nd in powder samples of $NdBa_2Cu_3O_{6+x}$ ($x = 0.94$, 0.78, 0.45, 0.3, 0.13). For our highest oxygen concentration, superconducting $NdBa_2Cu_3O_{6.94}$, we found that the Nd ions develop 3D long-range magnetic order at $T_N \simeq 0.53$ K, with spins coupled antiferromagnetically along the a, b, and c directions and the moment aligned along c.[7] The two experimental techniques at our disposal allow us to observe the manifestations of this long-range magnetic order in two forms: a sharp specific-heat anomaly, and resolution-limited magnetic Bragg peaks via neutron scattering. As we remove oxygen from this sample to arrive at partially deoxygenated superconducting $NdBa_2Cu_3O_{6.78}$, long-range order never develops down to the lowest temperatures achieved ($T = 0.3$ K). Indeed, a rounded magnetic specific-heat peak is observed, while neutron scattering reveals a broad, asymmetric line shape to the magnetic scattering which we can model with a 2D theory assuming short-range correlations. A further reduction of oxygen to insulating $NdBa_2Cu_3O_{6.45}$ does not restore long-range order, though the magnetic scattering now indicates correlations along the c axis. With further reduction to $NdBa_2Cu_3O_{6.3}$, we find that long-range order has been restored, as evidenced by a sharp specific-heat anomaly and resolution-limited magnetic Bragg peaks. The 3D configuration of spins is identical to what we observe in $NdBa_2Cu_3O_{6.94}$, but we find that the ordering temperature is more than three times higher than for $NdBa_2Cu_3O_{6.94}$, increasing to $T_N \simeq 1.5$ K, and the moment direction is now canted off the c axis by $\approx 45°$. We note that preliminary results of our measurements on $NdBa_2Cu_3O_{6+x}$ have been reported earlier.[8]

II. EXPERIMENTAL CONDITIONS

The neutron experiments were performed at the research reactor at the National Institute of Standards and Technology on the triple-axis spectrometers BT-9 and BT-2. The scattering data were taken with a wavelength of 2.35 Å, which corresponds to an incoming neutron energy of $E_i = 14.8$ meV, and a pyrolytic graphite monochromator and filter. Both a He^3 and He dilution refrigerator were used for the low-temperature measurements. The $ErBa_2Cu_3O_{6+x}$ with $x \approx 0$, and $x \approx 0.6$ single crystals were prepared using a modified self-flux technique.[9] The as-grown single crystals were annealed in N_2 at 600 °C for about a week to reduce the oxygen content to $ErBa_2Cu_3O_{6+x}$ ($x \approx 0$). SQUID magnetometer measurements on the annealed crystal revealed no diamagnetic signal down to 4.2 K. The same crystal was later annealed in O_2 at 900 °C for about 2 h, and cooled to 500 °C at the rate of 50 °C/h, then very slowly cooled to room temperature at an average rate of 0.6 °C/h to achieve $x \approx 0.6$. SQUID magnetometer measurements on this crystal revealed a superconducting transition $T_c \simeq 75$ K. The preparation of the fully oxygenated $ErBa_2Cu_3O_7$ ($x \simeq 1, T_c = 92$ K) single crystal has been described in a previous article.[6]

The growth technique for the $DyBa_2Cu_3O_{6+x}$ single crystals has been described in a previous article.[10] The measured superconducting transition temperature for the fully oxygenated $x \simeq 1$ crystal was $T_c \simeq 90$ K, while that for our $x \simeq 0.54$ powder sample was $T_c \simeq 50$ K. We have made measurements on several different Dy123 single-crystal samples, ranging in weight from 2 to 250 mg, as well as a 13-g powder sample. A neutron profile refinement at a wavelength of 1.5453 Å and collimation of 10′-20′-10′ was done on the BT-1 powder diffractometer to establish the oxygen stoichiometry of the Dy powder sample.

The preparation of the $NdBa_2C_3O_{6+x}$ powder sample has been described in detail in a previous article.[5] A polycrystal sample was chosen so that the oxygen content could be readily determined and varied. A neutron profile refinement was done to establish the oxygen stoichiometry of the powder. The lowest achievable oxygen concentration for this sample was $x = 0.13 \pm 0.02$, which results in partial occupation of the interchain O(5) site by oxygen.[11] The superconducting transition for $NdBa_2Cu_3O_{6.94}$ was $T_c \simeq 92$ K, while that of $NdBa_2Cu_3O_{6.78}$ was $T_c \simeq 63$ K.

III. EXPERIMENTAL RESULTS ON $ErBa_2Cu_3O_{6+x}$

A. Fully oxygenated superconducting $ErBa_2Cu_3O_7$

We have discussed in previous articles[6] our study of the 2D and 3D magnetic behavior of fully oxygenated superconducting $ErBa_2Cu_3O_7$ using neutron-scattering techniques, so we will only briefly summarize our results here. Our measurements were made in the $(h\ 0\ l)$ scattering plane, where a rod of diffuse scattering is observed just below $T = 1$ K, which is due to the 2D short-range magnetic correlations of Er spins. Below $T_N = 0.62$ K the sublattice magnetization, which is a measure of the thermodynamic order parameter, is found to obey Onsager's exact solution of the 2D $S = \frac{1}{2}$ Ising model.[12,13] The indexing of the 3D magnetic Bragg peak for the $ErBa_2Cu_3O_7$ crystal used in this study is of the $(\frac{1}{2}0\frac{1}{2})$ type, which corresponds to a ground-state spin configuration characterized by spins coupled antiferromagnetically along both the a and c directions, and ferromagnetically coupled spins along the b direction, with

the moments lying along b (see Fig. 1). This is the only spin configuration we have observed with this sample.

B. Partially de-oxygenated superconducting $ErBa_2Cu_3O_{6.6}$

Now we turn to our partially deoxygenated single crystal which we shall refer to as $ErBa_2Cu_3O_{6.6}$. The sample is in the superconducting orthorhombic phase with an approximate oxygen concentration of $x \approx 0.6$. In Fig. 2, we show a low-temperature scan through the resolution-limited 3D magnetic Bragg peak, indexed as $(\frac{3}{2},0,0)$, measured on the $ErBa_2Cu_3O_{6.6}$ crystal. This indexing is appropriate for spins aligned antiferromagnetically along the a axis, and ferromagnetically along the b and c directions. We have also determined the moment to be along the crystallographic b direction, as expected. Again this is the only ground-state configuration we observe in this sample, and this is a different single crystal than the one in which we observed the $(\frac{1}{2}\ 0\ \frac{1}{2})$ structure. We do not believe the different magnetic structures are due to the differing oxygen concentrations, since in fully oxygenated powder samples of our own, in the powder and single crystals of Chattopadhyay *et al.*,[14] and the single crystals

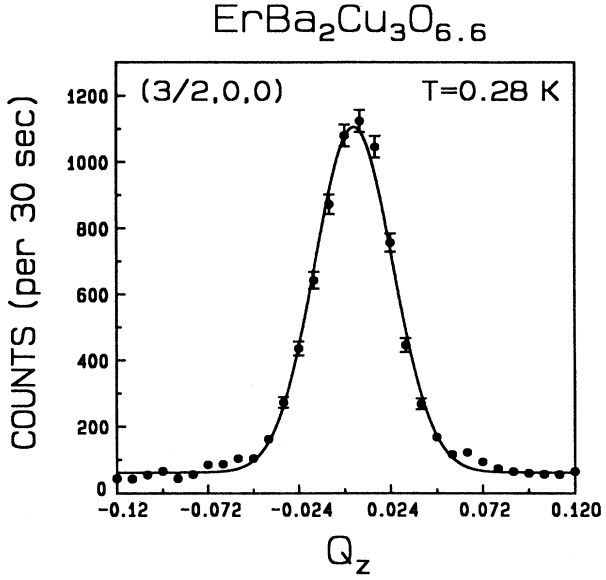

FIG. 2. 3D magnetic Bragg peak $(\frac{3}{2}\ 0\ 0)$ measured well below the ordering temperature, $T_N \simeq 0.48$ K, in partially deoxygenated superconducting $ErBa_2Cu_3O_{6.6}$.

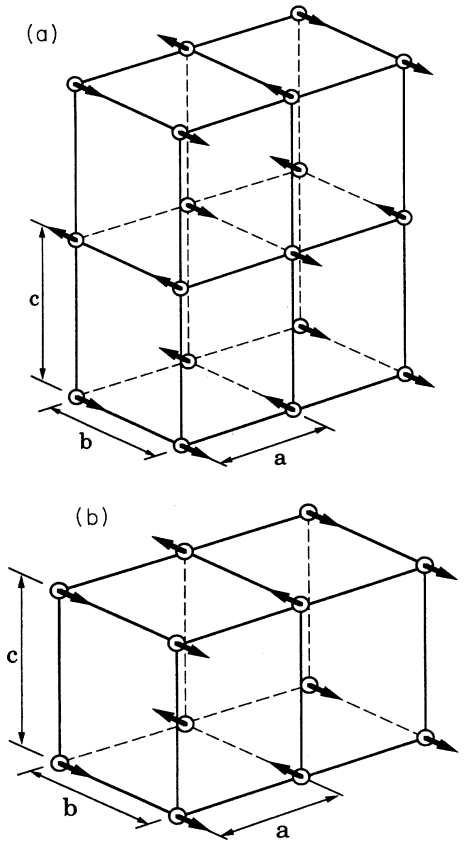

FIG. 1. Observed spin structures of $ErBa_2Cu_3O_{6+x}$. (a) Magnetic unit cell and 3D spin structure corresponding to $(\frac{1}{2}\ 0\ \frac{1}{2})$ indexing of magnetic Bragg peaks and (b) spin structure corresponding to $(\frac{1}{2}\ 0\ 0)$ indexing. We observe the $(\frac{1}{2}\ 0\ 0)$ structure in our $ErBa_2Cu_3O_{6.6}$ crystal.

of Paul *et al.*,[15] peaks with integer l are seen. The two possible Er spins structures are shown in Fig. 1.

In Fig. 3(a), we show a scan across the rod through the rod point $(\frac{1}{2}\ 0\ 0.3)$ at a temperature just above the 3D ordering temperature $T_N \approx 0.48$ K. This diffuse scattering is due to 2D short-range magnetic correlations in the a-b plane. The solid curve is a least-squares fit to a Lorentzian convoluted with the Gaussian resolution function. The Lorentzian shape of the intrinsic function is based on the Ornstein-Zernike approximation for the spin-spin correlation function. The diffuse magnetic scattering is then given by the spin-spin correlation function

$$\left[\frac{d\sigma}{d\Omega}\right]_{\text{diffuse}} \propto \langle S(-\mathbf{q})S(\mathbf{q})\rangle - \langle S(-\mathbf{q})\rangle\langle S(\mathbf{q})\rangle \propto (q^2+\kappa^2)^{-1} . \quad (1)$$

The half width at half maximum (HWHM) of the Lorentzian κ $(=1/\xi)$ is the 2D inverse correlation length, $\mathbf{q}=q_x\hat{a}^*+q_y\hat{b}^*=Q_x\hat{a}^*+Q_y\hat{b}^*-\tau_{2D}$, and τ_{2D} is the 2D reciprocal-lattice vector, which for Er is given by $(\frac{1}{2}\ 0)$. By fitting these data with the Ornstein-Zernike form we are able to extract the 2D correlations in the system at a given temperature, and in this way we can observe the evolution of the correlations in the a-b plane. At T_N the 2D correlations are long range and the peak becomes resolution limited. This has been discussed in detail for $ErBa_2Cu_3O_7$,[16] as well as for prototypical 2D systems such as K_2NiF_4.[17] Also shown in this figure is a scan along the rod just above the ordering temperature. We see that the scattering intensity is independent of the momentum transfer Q_z along the c direction, indicating that there are essentially no correlations along the c axis in the system above T_N. Therefore we say that above T_N

the system exhibits *only* 2D short-range magnetic correlations in the *a-b* plane. We remark that this is qualitatively the same behavior we observe in fully oxygenated $ErBa_2Cu_3O_7$.

At the ordering temperature, when strong correlations develop in the *a-b* plane, even a very weak interaction along the *c* direction is enough to induce 3D long-range order (see discussions in Refs. 6 and 16–18). Therefore, below T_N, we measure the magnetic Bragg scattering at the 3D positions. The temperature dependence of the magnetic scattering for our partially deoxygenated $ErBa_2Cu_3O_{6.6}$ crystal is shown in Fig. 4, measured at the

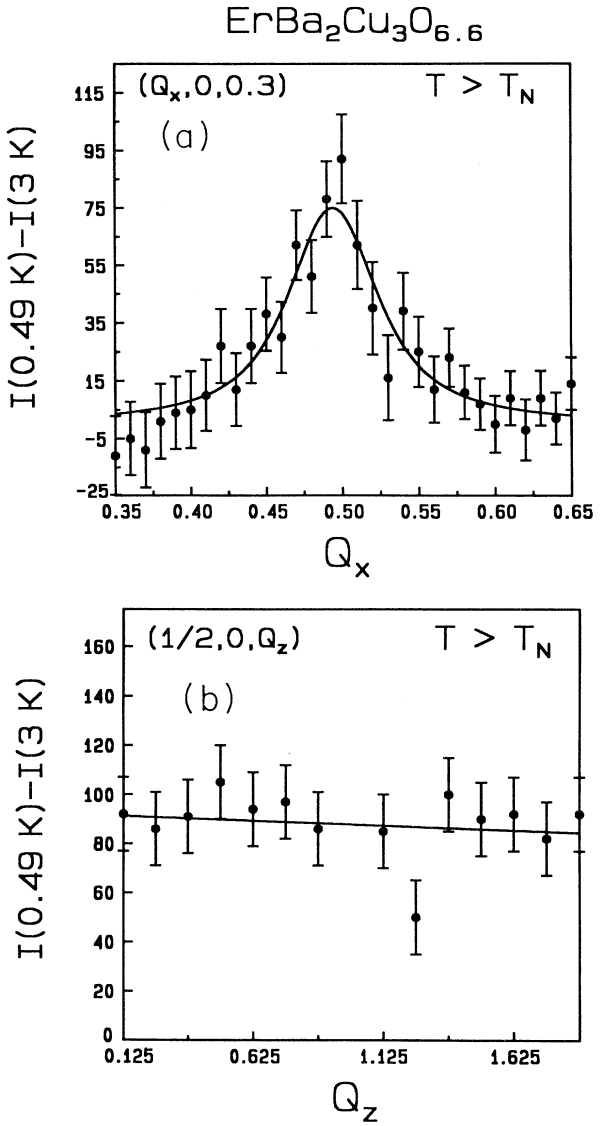

FIG. 3. (a) Scan across the rod of scattering in reciprocal space at the rod point ($\frac{1}{2}$ 0 0.3), showing the 2D character just above $T_N = 0.48$ K in $ErBa_2Cu_3O_{6.6}$. (b) A scan along the rod shows the scattering intensity does not vary significantly along Q_z, indicating there are no significant spin correlations between planes, even just above T_N. The slight decrease in intensity with increasing Q_z is due to the magnetic form factor.

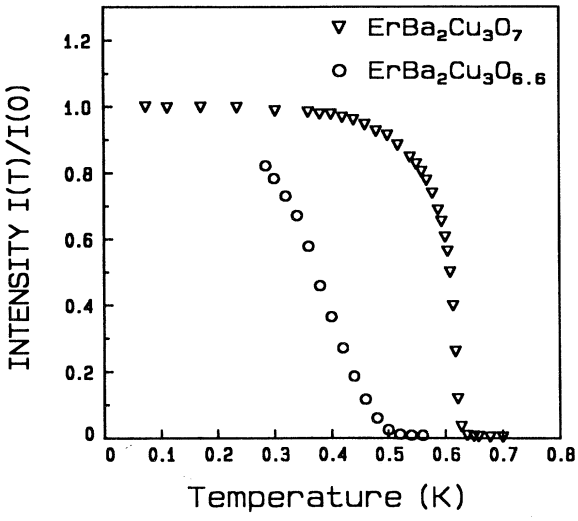

FIG. 4. Magnetic scattering intensity vs temperature measured at the ($\frac{1}{2}$ 0 0) 3D magnetic Bragg point on $ErBa_2Cu_3O_{6.6}$, $T_N \simeq 0.48$ K, as compared to measurements made on $ErBa_2Cu_3O_7$ at the ($\frac{1}{2}$ 0 $\frac{1}{2}$) 3D magnetic Bragg point, $T_N = 0.62$ K.

3D magnetic Bragg position ($\frac{1}{2}$ 0 0). We have also included in this figure the results for our fully oxygenated $ErBa_2Cu_3O_7$ crystal for comparison. From the figure we can see that the transition temperature in $ErBa_2Cu_3O_{6.6}$ has decreased markedly from that of $ErBa_2Cu_3O_7$. The transition is also notably broader, but we found a distribution of oxygen concentrations in this sample which we believe is creating this effect. In the fully oxygenated multicrystals of Paul *et al.*[15] they saw both the ($\frac{1}{2}$ 0 $\frac{1}{2}$) and ($\frac{1}{2}$ 0 0) structures, but with no discernible difference in the ordering temperatures of the two structures. Thus we believe the shift we observe in T_N is an oxygen effect. Indeed, the shift downward in transition temperature with decreasing oxygen concentration agrees qualitatively with the results of Maletta *et al.*[19] on Er123 powder samples, where they also found that the ordered moment had decreased. Unfortunately, for these measurements only the He^3 system was available, and thus we did not get to a low enough temperature to measure the fully ordered moment.

C. Insulating $ErBa_2Cu_3O_{6+x}$ ($x \approx 0$)

The results of our measurements on a nominally oxygenated $ErBa_2Cu_3O_{6+x}$ ($x \approx 0$) crystal are shown in Fig. 5. Figure 5(a) is a scan across the rod at our lowest achievable temperature (60 mK), and we see that the intensity peaks at the rod position. Again the solid curve is a least-squares fit to a Lorentzian intrinsic scattering function convoluted with the Gaussian resolution function, from which we find that even at this very low temperature this peak is not resolution limited. Indeed we extract a 2D correlation length of just 15 Å at this temperature, so that the system is exhibiting only short-range order. In Fig. 5(b), we show a scan along the rod also at

our lowest temperature, and we see that the diffuse intensity extended along Q_z is flat. In this scan we go through the 3D Bragg positions as well as points away from where the 3D Bragg points would lie, and yet there is no discernible change in the intensity. These results lead us to conclude that for $ErBa_2Cu_3O_{6+x}$ ($x \approx 0$) the Er spins exhibit *only* 2D short-range magnetic order down to $T = 60$ mK.

Finally, in Fig. 6 we have the temperature dependence of the diffuse magnetic scattering. The diffuse scattering develops below about 0.7 K, increasing continuously as we lower the temperature but never saturating down to our lowest achievable temperature of 60 mK. The 2D spin configuration which corresponds to the indexing of the 2D scattering vector is shown as an inset to Fig. 6. This is the same 2D spin configuration as seen in the oxygenated samples above their respective ordering temperatures, with the important difference that now $a = b$. From our measurements we are not able to determine the preferred moment direction, but presumably it is still in the a-b plane (see Simizu *et al.* in Ref. 2).

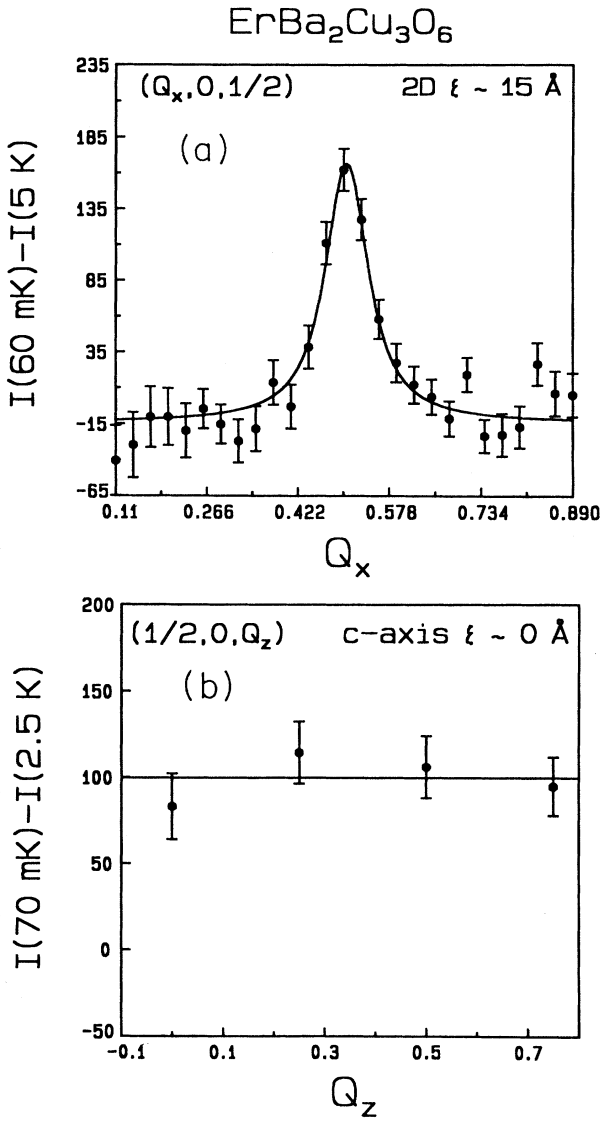

FIG. 5. (a) Scan across the rod at the rod point ($\frac{1}{2}$ 0 $\frac{1}{2}$) in nominally oxygenated insulating $ErBa_2Cu_3O_{6+x}$ ($x \approx 0$) at $T = 60$ mK. (b) A scan along the rod shows that the scattering intensity does not vary significantly along Q_z. The 2D correlations in the a-b plane are only short range, as we have determined $\xi \simeq 15$ Å at $T = 60$ mK.

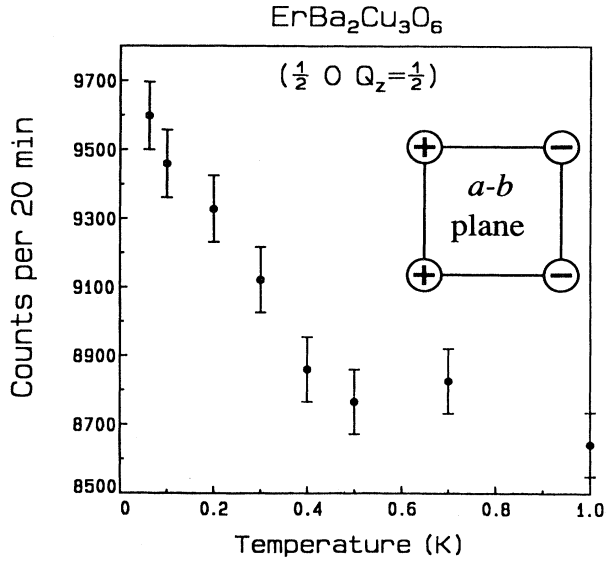

FIG. 6. Temperature dependence of the diffuse scattering in $ErBa_2Cu_3O_{6+x}$ ($x \approx 0$) measured at the rod position ($\frac{1}{2}$ 0 $\frac{1}{2}$). Down to $T = 60$ mK the scattering intensity does not saturate. Inset: the spin configuration in the a-b plane for tetragonal $ErBa_2Cu_3O_{6+x}$ ($x \approx 0$). This is also the lowest-energy spin configuration, with the moment lying in the plane, based on dipole energy considerations.

IV. THEORETICAL ANALYSIS: Er MAGNETIC DIPOLE INTERACTIONS

The low ordering temperature for the Er system suggests a rather weakly interacting system of spins. An appropriate model for the Er interaction may therefore be a simple dipole-dipole interaction. The total (ground-state) energy for a system of fully ordered point dipoles can be obtained by summing over the individual dipole-dipole interactions:

$$E = -\sum_{i}^{\text{all spins}} \sum_{j>i} \frac{3(\boldsymbol{\mu}_i \cdot \hat{\mathbf{r}}_{ij})(\boldsymbol{\mu}_j \cdot \hat{\mathbf{r}}_{ij}) - (\boldsymbol{\mu}_i \cdot \boldsymbol{\mu}_j)}{r_{ij}^3} . \quad (2)$$

Even though Eq. (2) assumes that the system is fully ordered (i.e., sufficiently low temperatures), a good order-of-magnitude estimate of the expected transition temperature can be made from it by finding the average energy per spin for N spins, E/N. We have made this calculation for $ErBa_2Cu_3O_7$ and its two possible spin configurations. We use the measured $\mu = 4.9\mu_B$ and $\boldsymbol{\mu} \| \hat{\mathbf{b}}$, $a = 3.82$ Å, $b = 3.88$ Å, and $c = 11.66$ Å, and find that the energy per spin converges very quickly (within 18% when summing over nearest neighbors only, and within 5% out

to next-nearest neighbors) to $\varepsilon \simeq -0.66$ K ($\simeq T_N$ in K) for both the ($\frac{1}{2}$ 0 $\frac{1}{2}$) and ($\frac{1}{2}$ 0 0) spin configurations. This is in good agreement with the experimentally determined ordering temperature of $T_N = 0.62$ K. Monte Carlo simulations of the Er order have been made assuming a 2D $S = \frac{1}{2}$ Ising antiferromagnet with dipole interactions,[20] where it is found that the ordering temperature is fairly close to the experimentally measured value, again indicating the importance of the dipole interaction.

Misra and Felsteiner have made detailed dipole calculations of the low-temperature (ordered) spin structure of Er in Er123 assuming dipole-dipole interactions, and they find that the two 3D structures observed (Fig. 1) are degenerate.[21] Since we observe only one structure or the other in a particular sample, this may indicate that the 3D spin structure in Er123 may be sensitive to defects in the samples such as the density of grain and twin boundaries, which somehow lift the degeneracy. The fact that both the ($\frac{1}{2}$ 0 0) and ($\frac{1}{2}$ 0 $\frac{1}{2}$) structures have been so readily observed in many different Er123 samples by various workers (our work as well as that of Refs. 14 and 15), indicates that the (dipole) degeneracy is the likely explanation.

As might be expected since $c \simeq 3a$, the contribution to Eq. (2) from spins in other layers is very small, indeed they are so small that the 3D structures characterized by ($\frac{1}{2}$ 0 0) and ($\frac{1}{2}$ 0 $\frac{1}{2}$) wave vectors are apparently degenerate. Thus we will treat only the two-dimensional Er spin system, as the 2D interactions are dominating the ordering. If we consider what happens when the system goes into its tetragonal phase, we put $a = b$ and then assume the moment direction is somewhere in the a-b plane. For an exchange-only magnetic system this would be well described by a 2D XY model. However, for a dipole system the a-b symmetry increases from twofold in the orthorhombic phase to fourfold in the tetragonal phase rather than to a continuous symmetry. With the moment in the 2D plane we find from Eq. (2) that the lowest-energy dipole spin configuration is that in Fig. 6, which is also the experimentally observed configuration. The dominant contribution to the average energy per spin, as determined by Eq. (2), comes from its four nearest neighbors in the a-b plane, and for the spins lying in the plane with the spin configuration as in Fig. 6 we have

$$\varepsilon_{nn} = -\frac{6\mu^2}{a^3}(1-2\cos^2\theta) , \tag{3}$$

where θ is the angle in the a-b plane between the moment direction and the axis along which the spins are coupled antiferromagnetically. From Eq. (3) we find that ε_{nn} has its minimum at $\theta = 90°$, when the moment lies along the axis with the spins coupled ferromagnetically as depicted in Fig. 7. Therefore, the angular dependence to ε_{nn} leads to an anisotropy in the plane, such that the moment prefers to be along the a, or equivalently along the b axis, and the moments coupled ferromagnetically along that direction.

The specific-heat data of Simizu *et al.*[2] in orthorhombic $ErBa_2Cu_3O_{6+x}$ ($x \gtrsim 0.3$) fit very nicely to a 2D $S = \frac{1}{2}$ Ising model, while in the tetragonal phase ($x \lesssim 0.3$) the specific-heat peak was significantly broadened and fit more effectively to an XY model. The authors suggested this may be due to the removal of the anisotropy in the a-b plane, so that the Er spin, which is locked along the b axis in the orthorhombic phase, becomes an XY spin in the tetragonal phase. Though the observation of a broad specific anomaly in tetragonal Er123 (Ref. 2) is consistent with the short-range order we observe in $ErBa_2Cu_3O_{6+x}$ ($x \approx 0$), from our analysis we see that the dipole interactions lead to a fourfold spin degeneracy rather than the continuous degeneracy of an XY model. Thus for the Er spins in tetragonal Er123, an XY model with continuous degeneracy is inappropriate. In theory the ground state of the dipole model is stable, and should exhibit long-range order at a temperature of the same order of magnitude as that for the 2D $S = \frac{1}{2}$ Ising model.[22] With this in mind it is surprising that short-range order persists in $ErBa_2Cu_3O_{6+x}$ ($x \approx 0$) down to temperatures which are more than an order-of-magnitude smaller than the T_N ($= 0.62$ K) in the 2D Ising like $ErBa_2Cu_3O_7$.

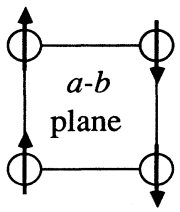

FIG. 7. The lowest-energy spin structure, with the moment in the plane, for dipole interactions. The fact that there is an easy axis for the moment direction rules out the possibility of the Er spins being described by an isotropic XY model in the tetragonal phase.

V. DISCUSSION OF THE Er RESULTS

Specific-heat results[2] indicate that the crystal-field ground state remains a doublet for $0 \lesssim x \lesssim 1$ in $ErBa_2Cu_3O_{6+x}$. Our own inelastic neutron-scattering experiments reveal that the lowest-energy crystal-field excitations are at 9.32 and 10.99 meV for the fully oxygenated sample, and they shift down to 7.06 and 10.97 meV for the fully deoxygenated system. The energy of the first excited state is large enough over the entire oxygen range that only the ground doublet should contribute appreciably to the free energy in the vicinity of T_N. Thus the Er^{3+} ions in $ErBa_2Cu_3O_{6+x}$ compounds can be treated as effectively $S = \frac{1}{2}$ particles over the entire oxygen range. However, we believe that further crystal-field measurements for more values of x in $RBa_2Cu_3O_{6+x}$, $0 \le x \le 1$, would be enlightening. Since the crystal-field ground state of the Er^{3+} ions is unaffected by oxygen concentration, the effects we observe must be due to changes in the magnetic interactions between Er ions.

Though the rare earths are likely electronically decoupled from the Cu-O planes on the order of T_c perhaps they are not decoupled on the order of T_N ($\ll T_c$). With this in mind, a Ruderman-Kittel-Kasuya-Yosida

(RKKY) indirect exchange interaction between Er ions is possible, and presumably would be affected by oxygen concentration. A RKKY interaction has also been proposed theoretically[23,24] to explain neutron-scattering measurements, on $ErBa_2Cu_3O_7$, for instance. However, there is still only limited experimental evidence that a RKKY interaction plays a role (Ref. 23, and references therein).

If there is an indirect coupling between the Er ions and the chain layer then the removal of oxygen could disrupt the Er spin interactions, reducing the average Er magnetic moment per site, and thus lowering the ordering temperature (recall from above $k_B T_N \simeq \varepsilon \propto \mu^2$). This will persist through the tetragonal phase where the Cu begins to order. The Cu order has not been considered to influence the rare earths in the 123 system, since the rare earths are believed to be at a symmetry site where all Cu magnetic interactions cancel. However, recent Mössbauer measurements on Er^{3+} diluted into $YBa_2Cu_3O_6$ indicate an anomalous molecular field of $B_{Cu(2)}=200$ G at the Er site due to the magnetic order of the Cu(2) in the Cu-O planes, and similar experiments on Yb^{3+} diluted into $YBa_2Cu_3O_6$ indicate an even larger field of $B_{Cu(2)}=1600$ G at the Yb site.[25] The size of the field at the Er site is about an order-of-magnitude smaller than the (saturated) Er dipole field, though the field found at the Yb site is about the same order of magnitude (comparing $\varepsilon_{nn}=-6\mu^2/a^3$ with $\mu \cdot B_{Cu(2)}$). With this range of field strengths observed at the rare-earth site it is possible that a Cu molecular field and the Er dipole field are competing interactions. This anomalous Cu molecular field, along with an indirect coupling of Er to the chain layer oxygen, may explain the diminishing magnetic order of Er as oxygen concentration decreases in $ErBa_2Cu_3O_{6+x}$.

VI. EXPERIMENTAL RESULTS ON $DyBa_2Cu_3O_{6+x}$

A. The 2D rod of magnetic scattering in Dy123

In our scattering experiments on single-crystal samples of Dy123 the measurements were made in the $(h\ h\ l)$ scattering plane. In Fig. 8, we present a diagram of reciprocal space, showing the positions of the 3D nuclear (crystal structure) and magnetic (spin structure) Bragg points, as well as the Bragg rods associated with 2D character. We have noted in this figure the positions of the magnetic Bragg points associated with the two oxygen-dependent spin structures. The rods of scattering extend along the (Q_z) direction in reciprocal space where the magnetic interactions are weakest, and thus the correlations along the c axis are inhibited. The anisotropy of the rare-earth magnetic unit cell, where nearest neighbors along the c direction are three times as distant as in the a-b plane, is the direct cause of the weak 3D interaction. Above the ordering temperature the rod intensity is due to short-range magnetic correlations in the a-b plane, while below T_N it arises from low-energy magnetic excitations.

In Fig. 9(a), we show a scan across the rod of magnetic scattering, just above the 3D ordering temperature ($T_N \approx 0.9$ K). These data are for a superconducting sample, and are typical of what we observe in our superconducting single crystals of $DyBa_2Cu_3O_{6+x}$. This strong rod of scattering develops for temperatures $\lesssim 2$ K, as will be discussed below. Since the HWHM of this peak is a direct measure of the inverse 2D correlation length κ, then by scanning across the rod at various temperatures we observe the evolution of the magnetic correlations in the a-b plane. Also shown in this figure is a scan along the rod, which demonstrates that the scattering intensity is independent of Q_z. Hence above T_N there are no significant correlations between spins in adjacent a-b planes, directly demonstrating that the c-axis interactions are very weak. The decrease in the scattering intensity Q_z we see in Fig. 9(b) is presumably due to the preferred c-axis alignment of the Dy spins, and the consequent suppression of the transverse magnetic fluctuations expected for an Ising-like system. There is also an additional fall off of intensity because of magnetic form factor effects.

B. Fully oxygenated $DyBa_2Cu_3O_7$ single crystals

Figure 10 shows the intensity versus temperature at a point on the rod $(\frac{1}{2}\ \frac{1}{2}\ 0.2)$ measured on our fully oxygenated superconducting sample $DyBa_2Cu_3O_7$. The rod starts to develop below about 2 K, and the intensity steadily increases with decreasing temperature until it

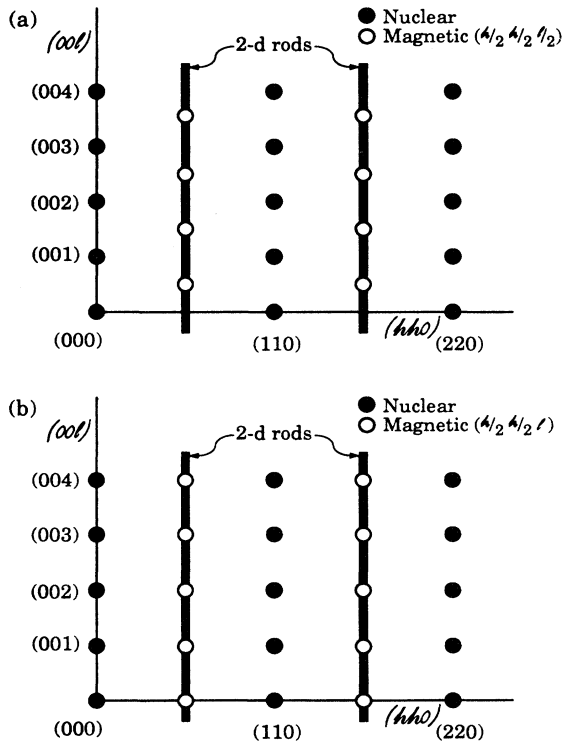

FIG. 8. (a) The scattering plane in reciprocal space showing the positions of 3D nuclear and magnetic Bragg points for the $(\frac{1}{2}\ \frac{1}{2}\ \frac{1}{2})$ configuration as well as the 2D magnetic Bragg rods. (b) The scattering plane showing the $(\frac{1}{2}\ \frac{1}{2}\ 0)$-type configuration of spins.

peaks at $T_N \simeq 0.93$ K, when long-range order sets in. Below T_N the intensity quickly decreases, presumably due to the sharp increase in the energy of the magnetic excitations, and the consequent decrease in their thermal population. This is what one would expect for an Ising-like system in which the transverse fluctuations are suppressed. Therefore, we may assume that the diffuse magnetic scattering intensity is primarily due to the longitudinal fluctuations of the Dy spins.

The temperature dependence of the inverse 2D correlations $\kappa(T)$ is shown in Fig. 11. Each data point is extracted from a scan across the rod similar to that shown in Fig. 9(a). The data values for κ have been obtained by a deconvolution of the measured width of the rod, where we assume a Gaussian resolution function folded with a Lorentzian intrinsic function. As discussed earlier, the intrinsic function is based on the Ornstein-Zernike approximation for the spin-spin correlation function, as given in Eq. (1). The correlation length ξ_{2D} $(=1/\kappa)$ grows continuously as the temperature is decreased, until at T_N the correlations are long range and the width of the rod is resolution limited. The solid curve is a fit to the power law $(T-T_N)^{0.9}$. The exponent $\nu=0.9$ is within 10% of the critical exponent for the 2D $S=\frac{1}{2}$ Ising model where in the limit $T \to T_N$, $\kappa \sim [(T-T_N)/T_N]^{\nu}$, with $\nu=1$. When strong correlations develop in the a-b plane, 3D long-range order is also induced, so that below T_N the elastic component of the magnetic scattering arises at 3D Bragg points characterized by the $(\frac{1}{2}\ \frac{1}{2}\ \frac{1}{2})$ wave vector, rather than a purely elastic component uniformly distributed along the rod.

The temperature dependence of the sublattice magnetization obtained from the $(\frac{1}{2}\ \frac{1}{2}\ \frac{1}{2})$ 3D magnetic Bragg

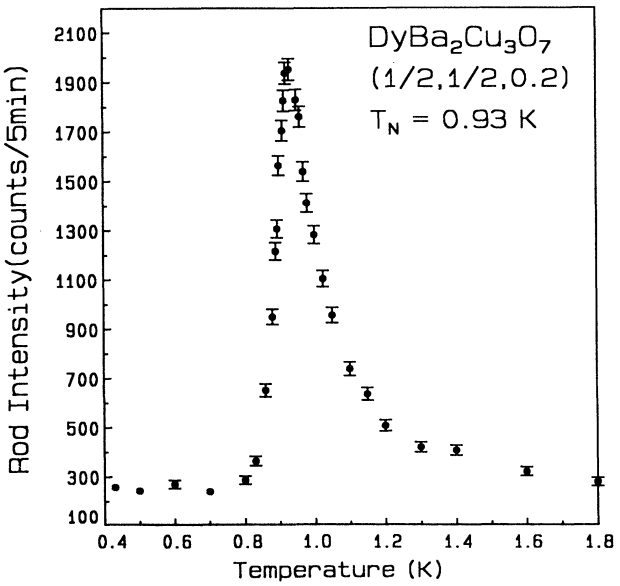

FIG. 10. Intensity of the rod of scattering as a function of temperature for a single crystal of fully oxygenated $DyBa_2Cu_3O_7$. The intensity is seen to peak at the ordering temperature $T_N \simeq 0.93$ K, where long-range correlations develop in the a-b plane.

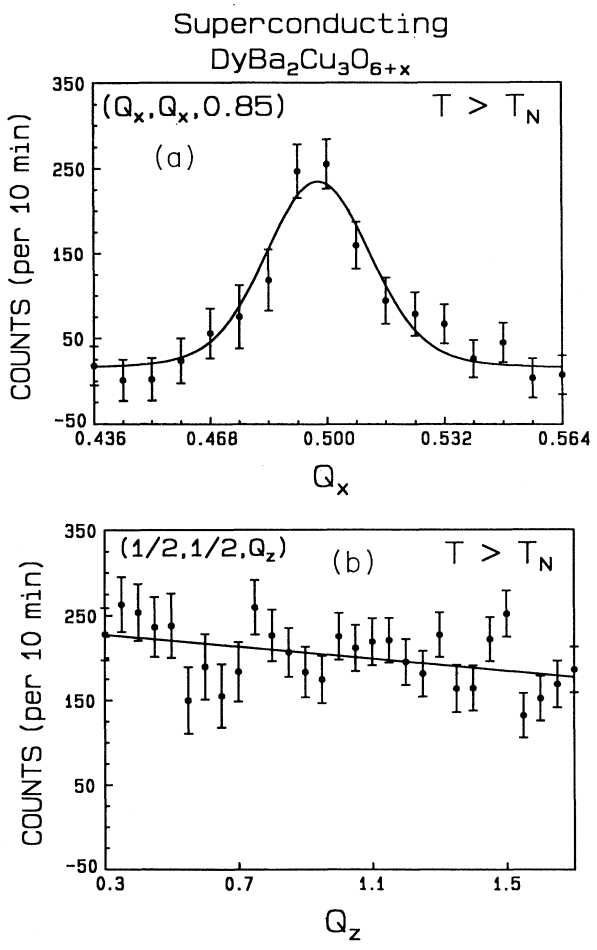

FIG. 9. (a) A scan across the rod of magnetic scattering in reciprocal space, showing the 2D character just above $T_N \cong 0.91$ K in a single crystal of superconducting $DyBa_2Cu_3O_{6+x}$ and (b) a scan along the rod, showing that the scattering intensity does not vary significantly along Q_z.

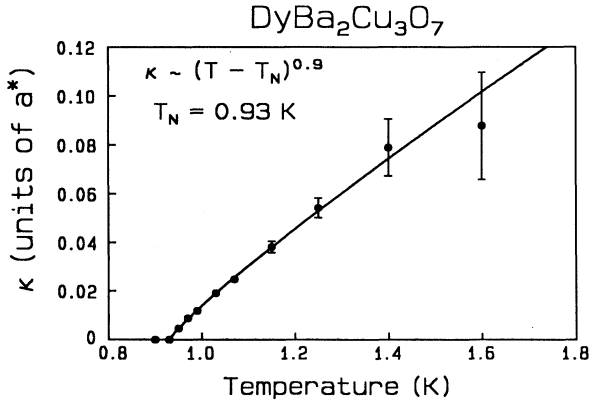

FIG. 11. The inverse correlation length vs temperature taken from measurements of the linewidth (HWHM) of the rod on a single crystal of fully oxygenated $DyBa_2Cu_3O_7$. The width of the rod becomes resolution limited at T_N where the correlations are long range.

peak is shown in Fig. 12. The curve is quite sharp, a characteristic of the 2D magnetic nature of the system. However, we do not find quantitative agreement with the order parameter for a 2D $S=\frac{1}{2}$ Ising model, in contrast to the behavior found in $ErBa_2Cu_3O_7$.[3,6,16] In fact, we have taken measurements on a number of other Dy123 samples, and we found even broader curves but in no case did we find a sharper curve. This is somewhat surprising since magnetic specific-heat measurements on $DyBa_2Cu_3O_7$ display a logarithmic divergence at the ordering temperature in agreement with the 2D $S=\frac{1}{2}$ Ising model. However, a small distribution of T_N's in the neutron samples may be spoiling the quantitative agreement with the 2D Ising model. The spin structure for this oxygen concentration is also depicted here, where the spins are coupled antiferromagnetically along all three crystallographic directions and the moment is along the c axis. This is the same spin structure determined in the neutron-scattering experiments of Goldman *et al.*[26] and Fischer *et al.*[27] on powder samples of fully oxygenated superconducting $DyBa_2Cu_3O_7$.

C. Oxygen dependence of the spin configuration

Our data reveal that the magnetic structure along the c axis changes from antiferromagnetic to ferromagnetic, depending on oxygen content. One might guess that the most likely concentration for the spin structure to change would be $x\approx 0.4$, where the system changes from metallic to semiconducting and where long-range magnetic order of the Cu moments occurs for $x\lesssim 0.4$. However, this turns out not to be the case, as we found that the structure had already changed at substantially higher x, in the superconducting regime.

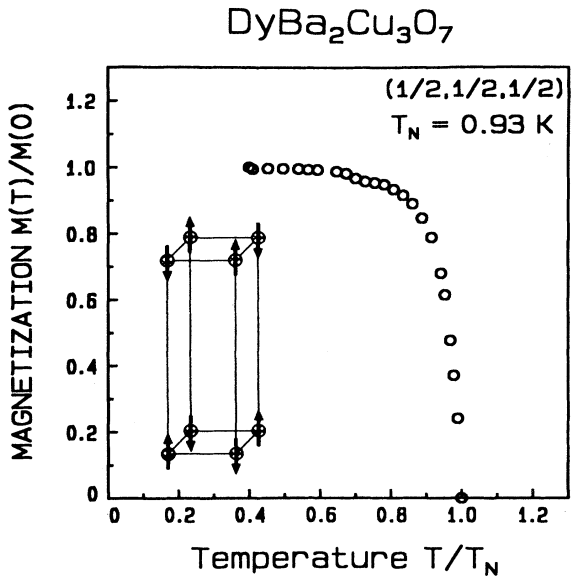

FIG. 12. (a) Sublattice magnetization vs temperature obtained from the $(\frac{1}{2}\ \frac{1}{2}\ \frac{1}{2})$ 3D magnetic Bragg peak, with $T_N\simeq 0.93$ K, measured on a single crystal of fully oxygenated $DyBa_2Cu_3O_7$. The 3D configuration of spins appropriate for this oxygen concentration is also shown.

To determine the oxygen concentration where the magnetic structure changes, we needed single crystals at intermediate x, with a uniform distribution of oxygen throughout the sample. Such uniformity turned out to be very difficult to obtain while controlling the value of x. We therefore decided to take data on a polycrystalline sample, where good oxygen uniformity could be readily obtained. The powder sample of $DyBa_2Cu_3O_{6+x}$ was made by the usual solid-state reaction techniques. The oxygen stoichiometry of the powder was established using thermogravimetric analysis (TGA). In addition, neutron powder diffraction data were obtained for one of the oxygen concentrations, and a full profile refinement was carried out to determine the absolute value of x. We obtained $x=0.54\pm 0.03$ for the sample with a measured T_c of 50 K. This refinement unambiguously established the oxygen content, and was in fact in excellent agreement with the TGA results starting from a "fully" oxygenated sample of $x=0.99\pm 0.04$ (TGA).

In Fig. 13(a), we show an angular scan at low temperature taken on this superconducting ($T_c\simeq 50$ K) $DyBa_2Cu_3O_{6.54}$ powder sample. In this angular range we observe the three magnetic Bragg peaks $(\frac{1}{2}\ \frac{1}{2}\ 0)$, $(\frac{1}{2}\ \frac{1}{2}\ 1)$,

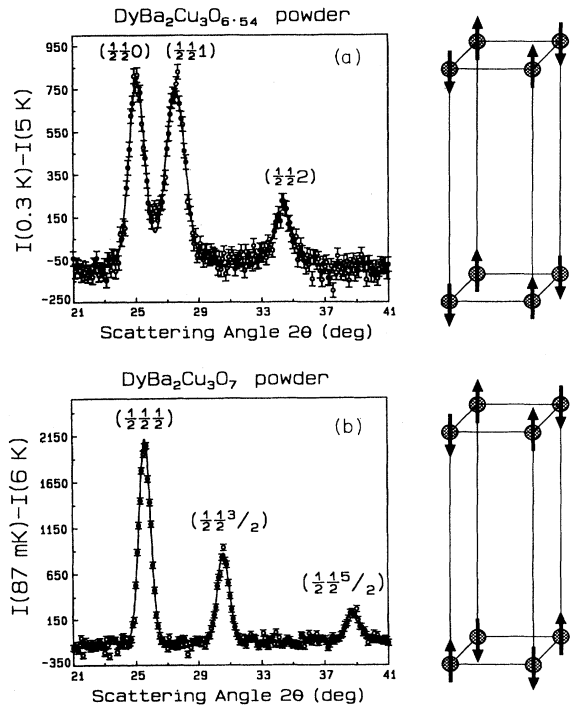

FIG. 13. (Top) Low-temperature angular scan through the 3D magnetic Bragg peaks $(\frac{1}{2}\ \frac{1}{2}\ 0)$, $(\frac{1}{2}\ \frac{1}{2}\ 1)$, and $(\frac{1}{2}\ \frac{1}{2}\ 2)$, made on a powder sample of superconducting $DyBa_2Cu_3O_{6.54}$ ($T_c\simeq 50$ K). The integral values for l signify that nearest-neighbor spins along the c axis are parallel. (Bottom) An identical low-temperature scan taken after annealing the sample in O_2 to get fully oxygenated $DyBa_2Cu_3O_7$. The Bragg peaks now arise at the $(\frac{1}{2}\ \frac{1}{2}\ l/2)$ positions (l odd), corresponding to antiferromagnetic spins along c. The appropriate spin structure is displayed to the right of its corresponding graph.

and $(\frac{1}{2}\ \frac{1}{2}\ 2)$, corresponding to spins coupled antiferromagnetically along the a and b directions, and ferromagnetically along the c axis. The spin structure is shown to the right, where we have determined the moment direction to be along the c axis just as for the fully oxygenated case. For comparison we show in Fig. 13(b) the same low-temperature angular scan taken on this powder after being annealed in O_2, increasing the oxygen concentration to $x \simeq 1$ ($DyBa_2Cu_3O_7$) and the superconducting transition to $T_c \simeq 90$ K. Now we see the three magnetic Bragg peaks $(\frac{1}{2}\ \frac{1}{2}\ \frac{1}{2})$, $(\frac{1}{2}\ \frac{1}{2}\ \frac{3}{2})$, and $(\frac{1}{2}\ \frac{1}{2}\ \frac{5}{2})$ corresponding to antiferromagnetically coupled spins along the c axis. Therefore, we see that removing oxygen changes the spin coupling along the c axis from antiferromagnetic to ferromagnetic while the system is still in the superconducting phase. These data establish that the magnetic structure changes in the range $0.54 < x < 1$, though we have not determined the precise concentration where this change occurs.

As discussed above, in Fig. 9 we showed measurements of the rod made on a single crystal of superconducting $DyBa_2Cu_3O_{6+x}$. An analogous measurement on our $DyBa_2Cu_3O_{6.54}$ powder sample is shown in Fig. 14, where we show the magnetic scattering profile above the ordering temperature. The solid curve is a least-squares fit to a 2D model, which assumes there is a rod of magnetic scattering characterized by the 2D wave vector $(\frac{1}{2}\ \frac{1}{2})$. The model will be discussed in detail in a latter section, when we present our powder data on the Nd system. We are above the 3D T_N where the spins are only correlated in the plane, and thus the (2D) spin configuration is the same as at the higher oxygen concentrations.

D. Effects of oxygen on the ordering temperature

We also find that creating oxygen vacancies in the chain layer lowers the ordering temperature. This is clearly illustrated in Fig. 15, where we contrast the order parameter determined from the $(\frac{1}{2}\ \frac{1}{2}\ \frac{1}{2})$ Bragg peak ($T_N \simeq 0.91$ K, $x \approx 1$) with that of the $(\frac{1}{2}\ \frac{1}{2}\ 0)$ peak

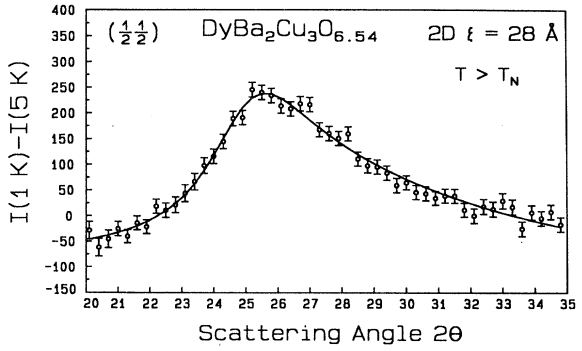

FIG. 14. Angular scan through the diffuse magnetic scattering just above the ordering temperature in the powder sample of superconducting $DyBa_2Cu_3O_{6.54}$. The solid curve is a fit to a 2D model which assumes a rod of scattering characterized by the 2D wave vector $(\frac{1}{2}\ \frac{1}{2})$. This is the powder sample analog of the single-crystal data in Fig. 9.

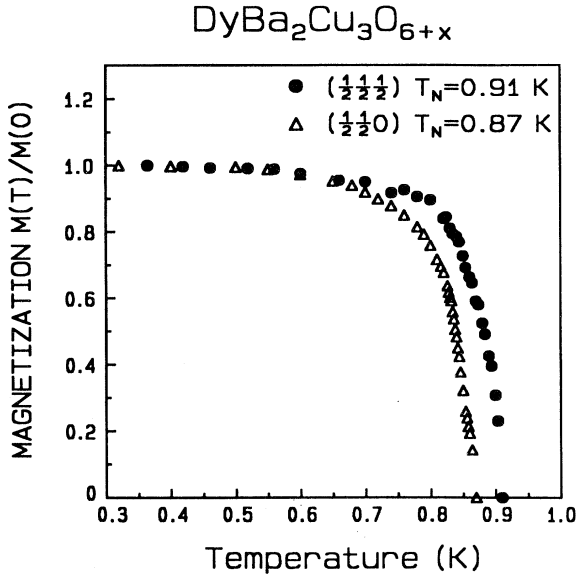

FIG. 15. Sublattice magnetization measured at the $(\frac{1}{2}\ \frac{1}{2}\ \frac{1}{2})$ 3D magnetic Bragg peak on a slightly deoxygenated superconducting single crystal of $DyBa_2Cu_3O_{6+x}$ with $T_N \simeq 0.91$ K, as compared to the measurement at the $(\frac{1}{2}\ \frac{1}{2}\ 0)$ 3D magnetic Bragg peak on a even more deoxygenated superconducting single crystal $DyBa_2Cu_3O_{6+x}$ with $T_N \simeq 0.87$ K. The data indicate that T_N decreases with decreasing oxygen content.

($T_N \simeq 0.87$ K, $x \approx 0.54$). These measurements were made on a single crystal of Dy123, and due to the difficult nature in making small changes in x on a crystal we were not able to establish the precise oxygen concentrations.

Hence we find that as we reduce the oxygen content both the spin configuration along the c axis and the ordering temperature are affected. In the nonsuperconducting phase, $x \lesssim 0.4$, we observe some additional changes in the 2D and 3D magnetic behavior of Dy, which we will address next.

E. Nonsuperconducting single crystals

We reduced the oxygen so as to study the magnetic order of Dy when the compound is in its nonsuperconducting phase. We made measurements on a nonsuperconducting single crystal at $x \approx 0$, and there is strikingly different magnetic behavior of the Dy ions from what we observed in the superconducting phase. We found slight decreases in the ordering temperature ($\approx 6\%$) as we removed oxygen in the superconducting phase, but a more substantial suppression of the ordering with decreasing x is found to occur in the nonsuperconducting phase.

The best way to appreciate the intrinsically different magnetic behavior is to compare the measurements of the rod in Fig. 9 made on superconducting $DyBa_2Cu_3O_{6+x}$ ($x > 0.4$), just above T_N(3D), with similar scans made on $DyBa_2Cu_3O_{6+x}$ ($x \approx 0$) displayed in Fig. 16. The scans across the rod in Figs. 9(a) and 16(a) are quite similar, and they reveal that all the Dy123 compounds exhibit strong 2D correlations above their respective ordering

temperatures. However, in Fig. 9(b) the scattering intensity along the rod is flat, indicating that there are essentially no correlations along the c-axis above T_N for superconducting $DyBa_2Cu_3O_{6+x}$ ($x > 0.4$), while in Fig. 16(b) we see broad peaks at the $(\frac{1}{2}\ \frac{1}{2}\ l)$ positions, with l an integer, indicating that there are considerably stronger, though still short-range, correlations along the c direction above T_N in the $DyBa_2Cu_3O_{6+x}$ ($x \approx 0$) compound. Even at our lowest temperature of $T = 70$ mK the widths of these 3D peaks, via a scan along the rod, as in Fig. 16(b), are about an order-of-magnitude larger than the resolution limit, while the widths derived from scans across the rod, as in Fig. 16(a), become resolution limited just below $T = 0.6$ K. This is in sharp contrast to what occurs in the superconducting compounds, where a scan along the rod reveals resolution-limited magnetic Bragg peaks at low temperatures [$T < T_N(3D)$]. Again, there is the expected decrease in the scattering intensity for increasing Q_z in Fig. 16(b), which is presumably due to the preferred c-axis alignment of the Dy spins, and the consequent suppression of the transverse magnetic fluctuations expected for an Ising-like system. There is also the additional fall off of intensity due to magnetic form-factor effects.

We have measured the temperature dependence of the HWHM of the peak shown in Fig. 16(a), and the results are shown in Fig. 17(a). The data are the deconvolution of the measured width of the rod, where we assume a Gaussian resolution function folded with a Lorentzian intrinsic function as previously done. We know from Eq. (1) that this is the temperature dependence of the inverse 2D correlation length κ. Significant 2D correlations develop below about 2 K, and grow continuously until at $T \simeq 0.55$ K long-range correlations develop in the a-b plane, as is evidenced by resolution-limited peaks. The solid curve is a fit to the power law $\kappa \sim (T - T_N)^1$, which is in good agreement with that expected for a 2D system as mentioned earlier.

In Fig. 17(b), we show the temperature dependence of the inverse correlations along the c direction, where the data were extracted from scans along the rod such as in

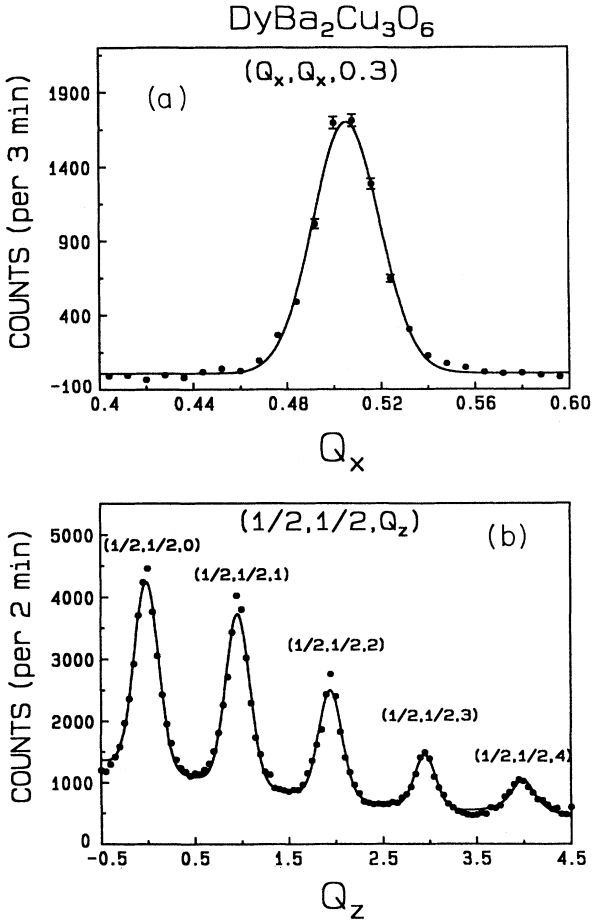

FIG. 16. (a) Scan across the rod, near the 2D ordering temperature $T_N(2D) \simeq 0.55$ K, taken on a nominally oxygenated single crystal of nonsuperconducting $DyBa_2Cu_3O_{6+x}$ ($x \approx 0$). (b) Scan along the rod at a temperature near $T_N(2D)$. The 3D peaks develop on the rod below about 2 K, indicating that there are 3D correlations in the system before 2D long-range order in the a-b plane ever occurs.

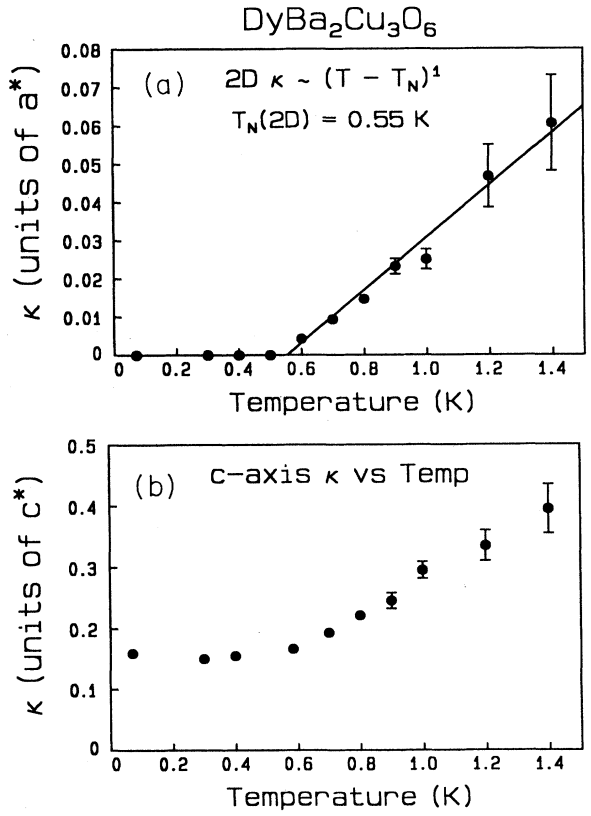

FIG. 17. (a) Temperature dependence of the 2D inverse correlations as measured on the nonsuperconducting $DyBa_2Cu_3O_{6+x}$ ($x \approx 0$) single crystal. The data are extracted from scans across the rod as in Fig. 16(a). The solid curve is a fit to the power law $(T - T_N)^1$ with $T_N = 0.55$ K. (b) Temperature dependence of the c-axis inverse correlations. The data are extracted from scans along the rod (i.e., along Q_z). The low-temperature c-axis correlation length is $\xi_{c\ \mathrm{axis}} \approx 13$ Å ($\approx c = 11.85$ Å).

Fig. 16(b). The correlations along the c direction appear just below 2 K, and grow continuously, until at $T=0.55$ K they saturate at $\xi_{c\text{-axis}}\approx 13$ Å when 2D long-range correlations develop in the a-b plane. The fact that 3D long-range order never develops in this compound, even though the correlations in the plane are long range, is quite unexpected. The behavior is at variance to that of all known "2D magnets," in which 3D long-range order is induced as a necessary consequence of the onset of 2D long-range order. The only known exception to this is the Dy order in superconducting $Dy_2Ba_4Cu_8O_{16}$.[18] However, in this compound there is a geometric cancellation of interactions between c-axis layers, which together with the weak intrinsic c-axis coupling renders the *net* interaction along the c axis much smaller than all other "2D magnets." This is clearly not the case for $DyBa_2Cu_3O_{6+x}$ ($x\approx 0$). The fact that we observe correlations along the c axis above T_N indicates that the coupling between layers is somehow enhanced.

Finally, in Fig. 18 we show the temperature dependence of the magnetic scattering measured at the $(\frac{1}{2}\ \frac{1}{2}\ 0)$ position. At 1.6 K we observe weak diffuse scattering which gradually increases in strength as we lower the temperature through $T_N(2D)\simeq 0.55$ K, eventually saturating just below 0.3 K. If the magnetic scattering intensity was entirely diffuse in nature, then presumably it should saturate when the correlations saturate at $T\simeq 0.55$ K. Therefore, the increase in scattering intensity below $T=0.55$ K seems to indicate that there is 2D long-range magnetic order of the Dy spins developing at $T_N\simeq 0.55$ K.

VII. DISCUSSION OF THE Dy RESULTS

A. Comparison to specific-heat measurements

The specific-heat data of Nakazawa, Ishikawa, and Takabatake[2] and Lee *et al.*[28] on powder samples of $DyBa_2Cu_3O_{6+x}$ show a sharp magnetic specific-heat anomaly at $T\simeq 0.9$ K in the superconducting phase, indicative of long-range magnetic order, and a rounded specific-heat anomaly in the nonsuperconducting phase, indicating a change in the nature of the ordering. Even more recent work on powder samples of $DyBa_2Cu_3O_{6+x}$ by Allenspach, Maple, and Furrer[4] has shown that the specific-heat anomaly, though rounded at $x=0.34$ in agreement with Refs. 2 and 28, is sharp again at $x=0.1$, indicating that long-range magnetic order is restored by further removing oxygen. These results are consistent with our observations that for low oxygen concentrations a change in the Dy magnetic order occurs, as 3D long-range order no longer develops despite the development of 2D long-range order at $T_N(2D)\simeq 0.55$ K in the $x\approx 0$ Dy123 compound. We further point out that from the work of Nakazawa, Ishikawa, and Takabatake[2] the Dy crystal-field ground state does not appear to be affected by oxygen. Thus we conclude that the changes we observe must be explained in terms of changes in the way the Dy ions interact with one another.

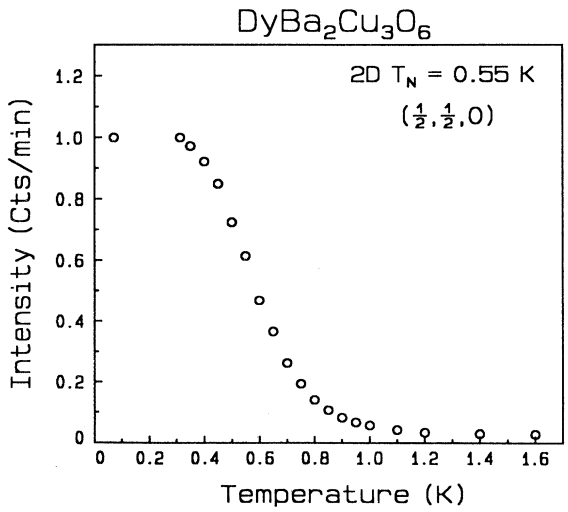

FIG. 18. Temperature dependence of the magnetic scattering at the $(\frac{1}{2}\ \frac{1}{2}\ 0)$ position on the rod, taken from the nominally oxygenated $DyBa_2Cu_3O_{6+x}$ ($x\approx 0$) single crystal.

B. Magnetic interactions of the Dy ions

Dipole-dipole interactions are expected to play a significant role in the intraplane interactions between Dy ions, as they are for many of the heavy rare-earth magnetic ions which have transition temperatures (≈ 1 K) of the same order of magnitude as their dipole energies [an exception is Nd and Sm (Refs. 3 and 5)]. As we have discussed earlier, a good order-of-magnitude estimate of the transition temperature can be made by finding the average dipole energy per spin for N spins. Such an estimate is only about 20% less than the observed $k_B T_N$. The dipole interactions between layers is expected to be much less important, as $c\simeq 3a$ leads to the 2D anisotropic behavior we observe. The lowest-energy 3D spin configuration for Dy, with its moment along the c axis, has antiparallel spins along a and b, and parallel spins along c, and is characterized by the $(\frac{1}{2}\ \frac{1}{2}\ 0)$-type wave vectors. This has been treated more thoroughly by Misra and Felsteiner[21] for all the rare-earth 3D spin structures in $RBa_2Cu_3O_{6+x}$ assuming dipole interactions alone, and their calculations agree with our more simplistic approach. However, all measurements indicate that the Dy moments are coupled antiferromagnetically along the c direction in $DyBa_2Cu_3O_7$,[10,26,27] thus showing a preference for a spin configuration with a slightly higher dipole energy. The dipole contribution from spins in other layers is very small, and we get nearly the same energy per spin for the $(\frac{1}{2}\ \frac{1}{2}\ 0)$ and $(\frac{1}{2}\ \frac{1}{2}\ \frac{1}{2})$ spin configurations. However, as small as the difference is ($\ll k_B T_N$), for ferromagnetic spins along c the energy contribution is negative, while for antiferromagnetic spins along c the energy is positive. This slight difference appears more significant if we consider why 3D long-range order is induced with the onset of 2D long-range order in the plane. When long-range order develops in the layers, then there is an energy $\pm J_c N$ between layers, where J_c is the energy of interaction along the c direction, and N is the average number of spins per domain in the layer. The minus sign is

for layers that are properly matched (e.g., ferromagnetic spins along c if $J_c > 0$) and the plus sign is for layers that are mismatched. Thus even if the interlayer coupling is very weak, there is an energy difference $\sim J_c N$ between the "correct" and the "wrong" spin configurations, and this energy can be quite large, since N is large. Hence as soon as 2D order is close to being established, an ordering should be induced along the c axis. Therefore, if dipole interactions were the dominant interaction between the layers, then we would not expect to observe the $(\frac{1}{2}\ \frac{1}{2}\ \frac{1}{2})$ spin configuration where spins are coupled antiferromagnetically along c. This suggests that there is a competing interaction (competing with an already weak dipole interaction) between Dy ions which favors an antiferromagnetic coupling along the c axis. In fact, Liu[24] has developed a model using a modified RKKY interaction involving electrons at energies away from the Fermi level, which can stabilize the three-dimensional magnetic order of the rare earth moments in $RBa_2Cu_3O_{6+x}$, and favors antiferromagnetism.

When oxygen is removed and we get to a yet undetermined concentration $0.54 < x < 1$ we find that the spins are coupled in their preferred dipole configuration of being parallel along c. Now the competing interaction appears to have lost out to the dipole interaction, indicating that the competing interaction is affected by oxygen vacancies. The oxygen vacancies in the lattice may also weaken the interactions in the plane enough to account for the lowering of T_N. And since we find that T_N falls off faster with x in the nonsuperconducting phase, where the Cu spins order, it is possible that the Cu order influences the Dy spins, as Mössbauer experiments on $ErBa_2Cu_3O_6$ and $YbBa_2Cu_3O_6$ (Ref. 25) have indicated that there is a weak anomalous Cu molecular field at the rare-earth site.

VIII. EXPERIMENTAL RESULTS ON $NdBa_2Cu_3O_{6+x}$

A. Neutron scattering

In Fig. 19, we show a low-temperature angular scan through the 3D magnetic Bragg peak $(\frac{1}{2}\ \frac{1}{2}\ \frac{1}{2})$ taken on our highest oxygenated superconducting $NdBa_2Cu_3O_{6.94}$ sample, while the inset displays the corresponding 3D spin structure for this oxygen concentration. All the observed magnetic Bragg peaks can be indexed by half-integral Miller indices. The indexing of the magnetic Bragg peaks indicates that the magnetic unit cell is doubled along all three crystallographic directions, and thus the spins are coupled antiferromagnetically along all three axes. The data were taken well below the ordering temperature of $T_N \simeq 0.53$ K, where the ordering is well developed. When 3D long-range order occurs we expect to see resolution limited 3D magnetic Bragg peaks below T_N, thus the solid curve through the data is a fit to the Gaussian resolution function. These measurements reproduce the results taken on polycrystalline $NdBa_2Cu_3O_7$ of Ref. 7.

For the $NdBa_2Cu_3O_{6+x}$ system all the measurements were carried out on powder samples in order to assure uniformity of oxygen. We now discuss the methods used

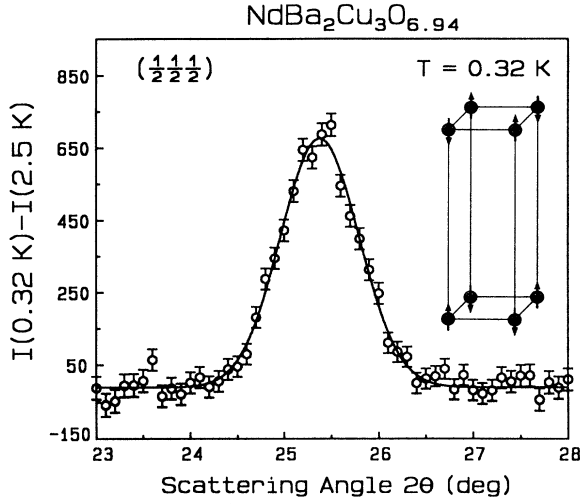

FIG. 19. Low-temperature angular scan through the 3D magnetic Bragg peak $(\frac{1}{2}\ \frac{1}{2}\ \frac{1}{2})$ measured on our highest oxygenated $NdBa_2Cu_3O_{6.94}$ sample. The solid curve is a fit to the Gaussian resolution, indicating that 3D long-range order has been reached. The inset shows the 3D ground-state spin structure.

to quantitatively analyze the powder data. Figure 20(a) shows a representative scattering plane for a system with 3D order. The solid points denote the Bragg points for the case of a single-crystal sample. To observe a single-crystal Bragg peak, we must have the scattering vector $\mathbf{Q} = \tau$ a reciprocal-lattice vector, that is, the neutron detector must be at the correct scattering angle $2\theta_{hkl}$ [with $\tau = (4\pi/\lambda)\sin\theta_{hkl}$], and the sample must be rotated to the proper orientation. A powder sample, on the other hand, consists of a large number of single crystals, randomly oriented. This has the effect of transforming each Bragg point into a Bragg sphere of radius τ, and the projection of these spheres onto the scattering plane yields a series of concentric circles as also shown in Fig. 20(a). The sample orientation is now irrelevant, and the measured Bragg angle $2\theta_{hkl}$ yields τ.

We have clearly demonstrated the 2D nature of the rare-earth magnetism in $DyBa_2Cu_3O_7$ and $ErBa_2Cu_3O_7$. For Nd we also expect the diffuse scattering above T_N to display dominantly 2D behavior. Thus, in Fig. 20(b) we show the positions of the Bragg rods associated with this 2D character. Note that in order to observe the rod, we can measure at any value of Q we like, as long as we scan through the rod, and as long as Q exceeds the minimum length $Q_{\min}$. For a powder, we must average over all possible orientations of reciprocal space. Note that unlike the 3D case, where the Bragg points define discrete spheres, the scattering from the rod is distributed over an infinite range in Q; there is a minimum ($Q_{\min}$) below which we will not observe any rod scattering, but there is no maximum. Thus, in the case of powder diffraction there will be a density of states associated with the rod scattering, as illustrated in Fig. 20(c). This situation was analyzed by Warren many years ago for the case of x-ray powder patterns of random layered materials.[29,18] In Fig.

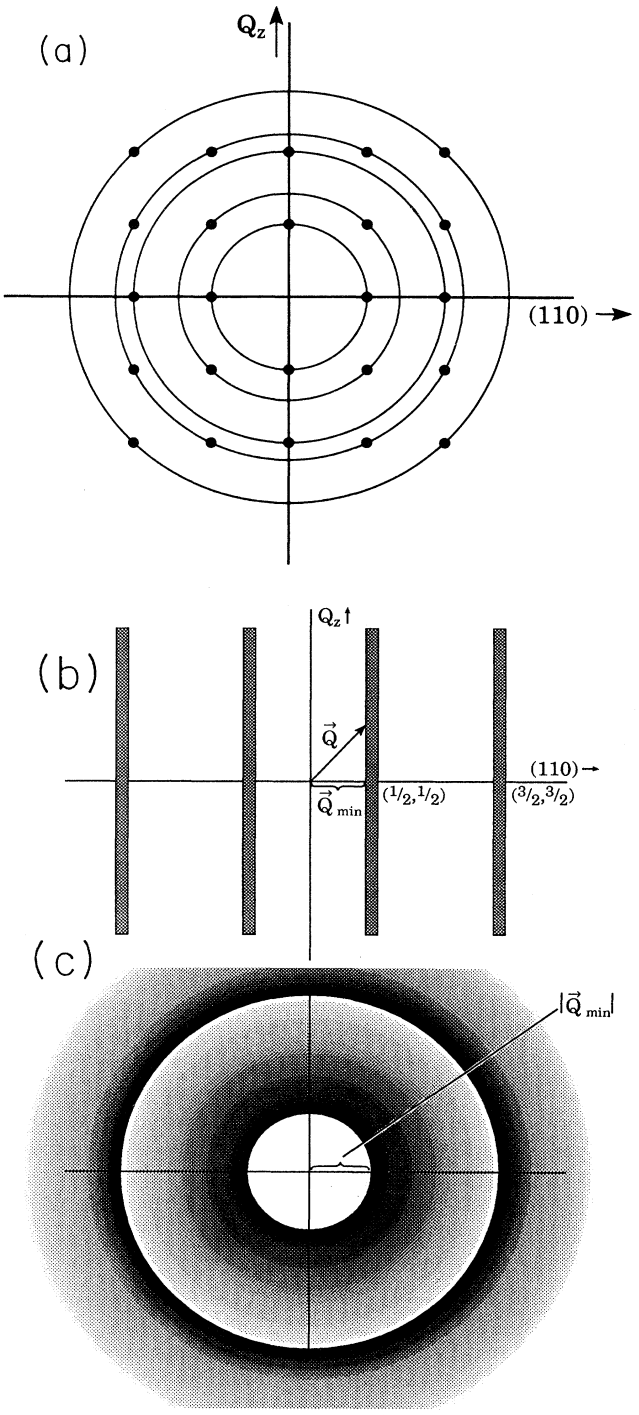

FIG. 20. (a) Schematic representation of the scattering plane, both for a single crystal, and for a powder. The solid points represent the 3D Bragg peaks for a single crystal. For a powder the Bragg intensities are distributed on spheres, which appear as circles in this scattering plane. (b) Schematic representation of the scattering plane for a 2D crystal, and (c) a 2D powder. For a powder the rods are transformed into a density of states for scattering.

21(a), we show a scattering profile just above the ordering temperature for $NdBa_2Cu_3O_{6.94}$. The solid curve is a least-squares fit to a 2D model, which assumes there is a rod of magnetic scattering characterized by the 2D reciprocal-lattice vector $\tau_{2D}=(\frac{1}{2}\ \frac{1}{2})$. To generate the fitted curve we use Warren's approach[29] of averaging the scattered intensity for a 2D powder over all possible orientations of reciprocal space, but here we assume the intrinsic line shape to the rod is Lorentzian rather than Gaussian as assumed in his case. This is appropriate for diffuse magnetic scattering where the 2D rod is propor-

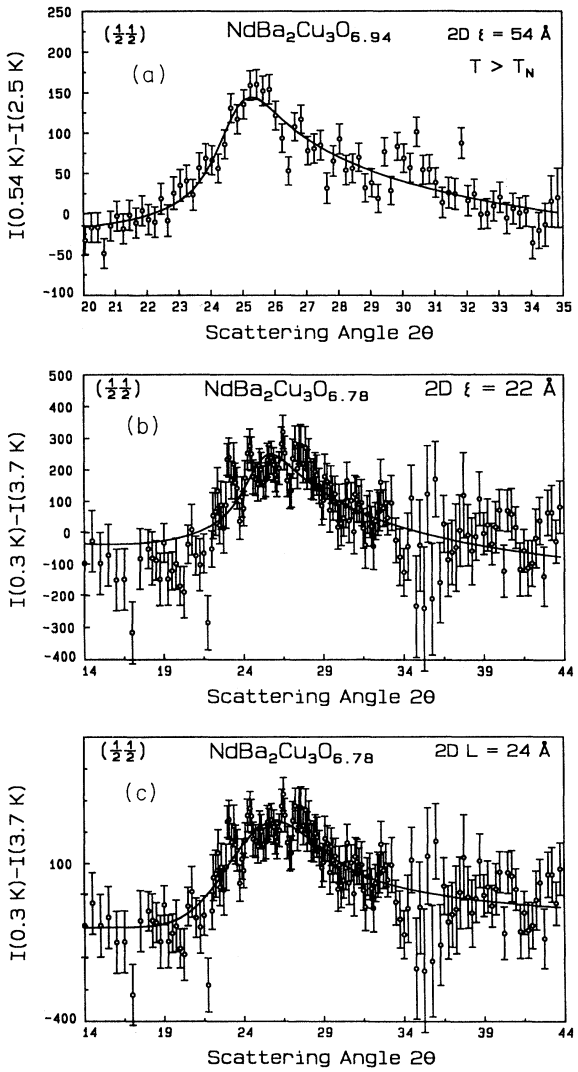

FIG. 21. (a) Angular scan through the diffuse scattering just above T_N in $NdBa_2Cu_3O_{6.94}$. The solid curve is a fit to a 2D model assuming short-range correlations. (b) A similar scan made at low temperature on partially deoxygenated superconducting $NdBa_2Cu_3O_{6.78}$. The low-temperature fitted 2D correlation length is only $\xi \simeq 22$ Å. (c) The data of (b) fit using a model which assumes the magnetic domains are small compared to the intrinsic spin-spin correlation length. In this model 2D magnetic domains with average length $L=24$ Å form down to low temperatures.

tional to the spin-spin correlation function, which in the Ornstein-Zernike approximation is given by Eq. (1). We then get for the scattering intensity

$$I_{hk}=\text{const}\times\frac{|F_M|^2}{\sin\theta}F(\theta)\ , \tag{4}$$

where 2θ is the scattering angle, F_M is the magnetic structure factor for the 2D magnetic unit cell,[18] and

$$F(\theta)=\int_{\text{Ewald sphere}}\frac{\kappa^2}{(q^2+\kappa^2)}\frac{dA}{\sin\theta} \tag{5}$$

represents the scattering from the rod summed over the surface of the Ewald sphere of radius Q. For convenience we make a change of variables $q^2=q_x^2+q_y^2=k_\parallel^2+k_\perp^2$, where $k_\parallel$ and $k_\perp$ are orthogonal variables such that $k_\parallel=(\mathbf{Q}-\tau_{2D})\cdot\hat{\tau}_{2D}$ is the component of $\mathbf{Q}-\tau_{2D}$ along $\hat{\tau}_{2D}$, which in the case of $NdBa_2Cu_3O_{6+x}$ is the (110) direction, as depicted in Fig. 20. We now approximate by replacing the Ewald spherical shell by the tangent cylindrical shell of radius Q and cylinder axis along the $k_\perp$ direction. This is a reasonable approximation since the integrand $\sim 1/k_\perp^2$. Equation (5) can now be written as

$$F(\theta)=\int_0^{\pi/2}\int_{-\infty}^{\infty}\frac{\kappa^2}{(k_\perp^2+k_\parallel^2+\kappa^2)}dk_\perp\frac{Qd\phi}{\sin\theta}\ . \tag{6}$$

The integral over $k_\perp$ can be carried out, and using $Q=(4\pi/\lambda)\sin\theta$, the fact that ϕ is the angle between $\mathbf{Q}$ and τ_{2D}, and

$$\begin{aligned}k_\parallel=(\mathbf{Q}-\tau_{2D})\cdot\hat{\tau}_{2D}&=Q\cos\phi-\tau_{2D}\\&=\frac{4\pi}{\lambda}(\sin\theta\cos\phi-\sin\theta_{hk})\end{aligned} \tag{7}$$

we get

$$F(\theta)=\int_0^{\pi/2}\frac{4\pi^2\kappa^2}{\lambda}\left[\frac{16\pi^2}{\lambda^2}(\sin\theta\cos\phi-\sin\theta_{hk})^2+\kappa^2\right]^{-1/2}d\phi\ , \tag{8}$$

where $2\theta_{hk}$ is the scattering angle where the Ewald sphere first intercepts the rod [i.e., $\tau_{2D}=(4\pi/\lambda)\sin\theta_{hk}$], λ is the neutron wavelength, and the integral is solved numerically. A finite correlation length will give the rods a certain "thickness," and this will manifest itself in the intrinsic Lorentzian character of the measured spin-spin correlation function. The fit in Fig. 21(a) is very good, indicating that just above T_N the 2D correlations are strong. This does not rule out the possibility of there being weak correlations along the c axis above T_N, as it is difficult to resolve the c-axis correlations in this type of measurement. However, if they exist they are not very pronounced, as there is no clear indication of peaks arising at the 3D positions in this angular range (the positions of relevant 3D peaks will be discussed below). Also shown in Fig. 21 is a measurement taken on our partially deoxygenated superconducting sample $NdBa_2Cu_3O_{6.78}$. Figure 21(b) is a scan taken at low temperature on this powder, and the solid curve is a least-squares fit to Eq. (4). Quite unexpectedly, we find at low temperatures, where the magnetic scattering has already saturated in intensity, that it is still *only* short range in nature, arising from 2D short-range magnetic correlations. The 2D correlation length we extract at $T=0.3$ K is only 22 Å. If the size of magnetic domains in the sample is comparable to or smaller than the intrinsic spin-spin correlation length, i.e., over the finite length scale of a magnetic domain the spins are correlated, then the rods will have a certain "thickness" which is Gaussian in its distribution. This is similar to the situation Warren considered for the case of x-ray powder patterns of layered materials,[29] and Zhang *et al.* considered for powder samples of the 2D magnetic system $Dy_2Ba_4Cu_7O_{15}$.[18] Warren's calculation[29] assuming a Gaussian line shape to the 2D rod yields

$$F(\theta)=\int_0^{\pi/2}\exp\left[-\frac{4\pi L^2}{\lambda^2}(\sin\theta\cos\phi-\sin\theta_{hk})^2\right]d\phi\ , \tag{9}$$

where L is a parameter that represents the size of a 2D magnetic domain:

$$L=[(1/N_xa)^2+(1/N_yb)^2]^{-1/2}\ , \tag{10}$$

and $(N_xa\times N_yb)$ is the area of a domain in the ab plane. In Fig. 21(c), we show the same data as in Fig. 21(b), with the important difference that here we have least-squares fit the data assuming a Gaussian shape to the 2D rod of scattering [Eqs. (4) and (9)]. We find from our fit that the 2D domain size at $T=0.3$ K is only $L=24$ Å, where we now assume the intrinsic 2D spin-spin correlation length ξ is large compared to the domain size L, i.e., $\xi\gg L$. The fits in Figs. 21(b) and 21(c) are very comparable, as we find from our least-squares fit that for the Lorentzian rod (domain size $L\gg$spin-spin correlation length ξ) $\chi=1.13$, and for the Gaussian rod (intrinsic spin-spin correlation length $\xi\gg$domain size L) the fit is slightly improved with $\chi=0.98$. Due to the weak nature of the magnetic scattering intensity from a sample with spins correlated over such small length scales, it is difficult to determine which model best represents the data. However, Allenspach, Maple, and Furrer[4] have had reasonable success fitting the Nd magnetic specific-heat data of partially deoxygenated superconducting $NdBa_2Cu_3O_{6.72}$ using a 2D spin cluster model, which assumes finite-size clusters, on the order of a few lattice spacings, of correlated spins (we will say more about the specific-heat results in a later section). This suggests that the finite-size magnetic domain model we used above may be more appropriate for the magnetic order of Nd in partially deoxygenated superconducting $NdBa_2Cu_3O_{6.78}$. We emphasize that this is not the appropriate model for our fully oxygenated sample, $NdBa_2Cu_3O_{6.94}$, above its ordering temperature, and this is evidenced by the fact that the fit in Fig. 21(a) assuming a Lorentzian line shape to the rod gives us a significantly better fit than we can achieve assuming a Gaussian line shape.

The temperature dependence of the magnetic scattering measured at the $(\frac{1}{2}\ \frac{1}{2}\ \frac{1}{2})$ position on the

$NdBa_2Cu_3O_{6.78}$ compound is shown in Fig. 22. The magnetic scattering develops at the relatively high temperature of 1.5 K, and is seen to saturate at about 0.4 K. It is rather remarkable that this magnetic scattering is now developing at temperatures about three times higher than observed in $NdBa_2Cu_3O_{6.94}$, even though long-range order never develops.

A low-temperature scan taken on the nonsuperconducting $NdBa_2Cu_3O_{6.45}$ sample is shown in Fig. 23(a), where we can now clearly resolve two peaks at the 3D Bragg positions $(\frac{1}{2}\ \frac{1}{2}\ \frac{1}{2})$ and $(\frac{1}{2}\ \frac{1}{2}\ \frac{3}{2})$. At this temperature the scattering intensity has already saturated, yet the two peaks are still considerably broader than the resolution. This indicates that the correlations along the c axis are considerably stronger than what we observed in $NdBa_2Cu_3O_{6.78}$, but 3D long-range order is still absent.

In Fig. 23(b), we show an angular scan, over the same angular range as in Fig. 23(a), taken at low temperatures on our sample with the lowest oxygen stoichiometry of $NdBa_2Cu_3O_{6.13}$. The important difference between these results and those of $NdBa_2Cu_3O_{6.45}$ is that in Fig. 23(b) the two peaks are resolution-limited magnetic Bragg peaks, indicating that long-range order of the Nd ions develops in this compound. However, the relative intensities of the $(\frac{1}{2}\ \frac{1}{2}\ \frac{1}{2})$ and $(\frac{1}{2}\ \frac{1}{2}\ \frac{3}{2})$ peaks differ from what we observed for the same peaks in $NdBa_2Cu_3O_7$,[7] where $\boldsymbol{\mu}\|c$. We also observe a strong $(\frac{1}{2}\ \frac{1}{2}\ \frac{5}{2})$ peak for the deoxygenated samples, which was quite weak in our $NdBa_2Cu_3O_7$ data. In fact, for $NdBa_2Cu_3O_{6.13}$ we can model the data very well if we assume the moment direction is off the c axis by 45°. We also find an ordered moment, $\langle \mu_z \rangle \simeq (0.85 \pm 0.04)\mu_B$, which is reduced by about 20% from what we estimate for $NdBa_2Cu_3O_7$ where $\langle \mu_z \rangle \simeq 1.1\mu_B$.[7] However, the Nd ordering in the insulating phase could be complicated by the Cu order, and may account for some of these differences. The experimental intensities and some calculated values are listed in Table I.

Finally, we show in Fig. 24 the temperature dependence of the magnetic scattering measured at the $(\frac{1}{2}\ \frac{1}{2}\ \frac{1}{2})$ position for two different oxygen concentrations, $NdBa_2Cu_3O_{6.13}$ and $NdBa_2Cu_3O_{6.94}$. From the figure we see that the transition temperatures differ by about a factor of 3, where for $NdBa_2Cu_3O_{6.13}$ we find $T_N \simeq 1.75$ K and for $NdBa_2Cu_3O_{6.94}$ $T_N \simeq 0.53$ K.

We have not made comparisons of the scattering data with any known model such as the 2D $S=\frac{1}{2}$ Ising model, as has been commonly done with the rare-earth order in $RBa_2Cu_3O_{6+x}$. As we have discussed in previous arti-

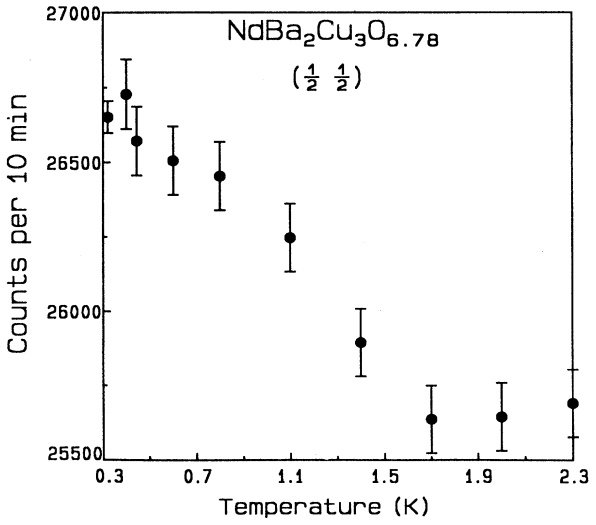

FIG. 22. Temperature dependence of the magnetic scattering in partially deoxygenated superconducting $NdBa_2Cu_3O_{6.78}$. The magnetic scattering develops at the relatively high temperature of 1.5 K, and the intensity saturates near 0.4 K.

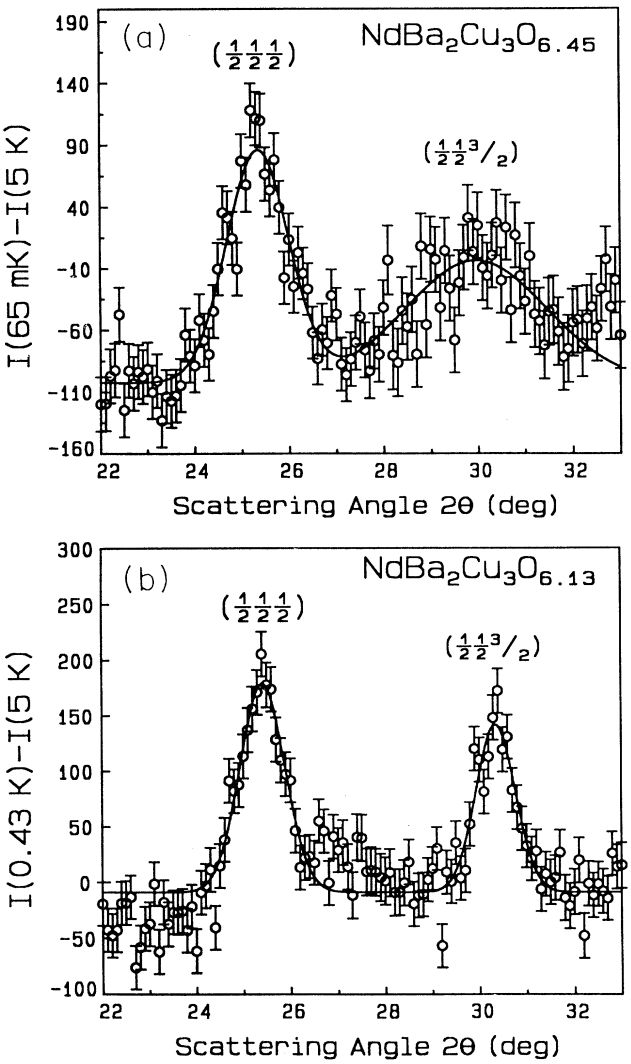

FIG. 23. (a) Low-temperature angular scan through two 3D magnetic peaks indexed as $(\frac{1}{2}\ \frac{1}{2}\ \frac{1}{2})$ and $(\frac{1}{2}\ \frac{1}{2}\ \frac{3}{2})$, on the nonsuperconducting $NdBa_2Cu_3O_{6.45}$ sample. The 3D correlations are only short range in nature. (b) A similar low-temperature scan taken on insulating $NdBa_2Cu_3O_{6.13}$. The data reveal sharp resolution-limited Bragg peaks, indicating that 3D long-range order is restored for this oxygen concentration.

TABLE I. Ratios of observed magnetic intensities for $NdBa_2Cu_3O_{6+x}$, compared to the calculated values assuming a particular spin direction. The assumption of the spins being off the c axis by 45° provides a better description of the data in $NdBa_2Cu_3O_{6.13}$, whereas the moment parallel to c describes the $NdBa_2Cu_3O_7$ data best (Ref. 7). The results on $NdBa_2Cu_3O_{6.3}$ are inconclusive, but we anticipate the same spin direction as in $NdBa_2Cu_3O_{6.13}$.

(hkl)	I_{obs}	I_{calc} (c axis)	I_{calc} (45° off c axis)
$NdBa_2Cu_3O_7$			
$(\frac{1}{2}\ \frac{1}{2}\ \frac{1}{2})$	$\equiv 1.00\pm0.03$	1.00	1.00
$(\frac{1}{2}\ \frac{1}{2}\ \frac{3}{2})$	0.40 ± 0.03	0.50	0.65
$(\frac{1}{2}\ \frac{3}{2}\ \frac{1}{2})$	0.23 ± 0.02	0.21	0.21
$NdBa_2Cu_3O_{6.3}$			
$(\frac{1}{2}\ \frac{1}{2}\ \frac{1}{2})$	$\equiv 1.00\pm0.09$	1.00	1.00
$(\frac{1}{2}\ \frac{1}{2}\ \frac{3}{2})$	0.59 ± 0.08	0.50	0.65
$NdBa_2Cu_3O_{6.13}$			
$(\frac{1}{2}\ \frac{1}{2}\ \frac{1}{2})$	$\equiv 1.00\pm0.07$	1.00	1.00
$(\frac{1}{2}\ \frac{1}{2}\ \frac{3}{2})$	0.61 ± 0.05	0.50	0.65
$(\frac{1}{2}\ \frac{1}{2}\ \frac{5}{2})$	0.46 ± 0.06	0.19	0.40

cles,[3,30] this is due to the nature of magnetic scattering in powder samples, where it is impossible to separate the elastic Bragg component of the scattering from the diffuse scattering without measuring the energy dependence. For instance, the thermodynamic order parameter (sublattice magnetization) is determined from the Bragg scattering, while the susceptibility is derived from the diffuse scattering. Since we are unable to separate the two components of the scattering, we are limited to observing the qualitative nature of the magnetic order. Future experiments made on single-crystal samples should circumvent this difficulty.[30]

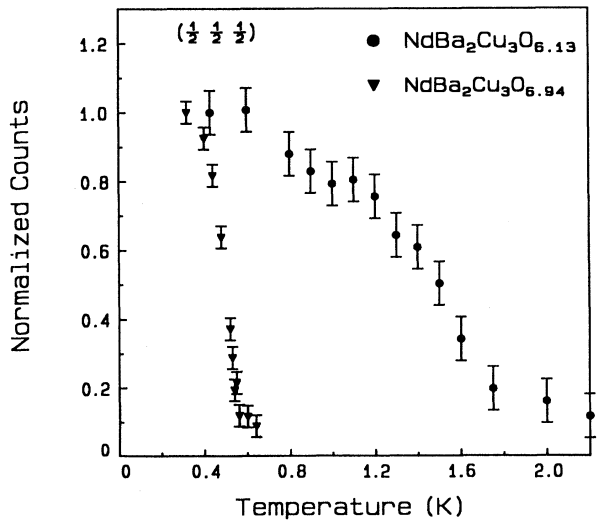

FIG. 24. Temperature dependence of the magnetic scattering intensity measured at the $(\frac{1}{2}\ \frac{1}{2}\ \frac{1}{2})$ Bragg peak for both $NdBa_2Cu_3O_{6.94}$ and $NdBa_2Cu_3O_{6.13}$. The ordering temperature for $NdBa_2Cu_3O_{6.13}$ ($T_N \simeq 1.75$) is more than three times higher than that in $NdBa_2Cu_3O_{6.94}$ ($T_N \simeq 0.53$ K).

B. Specific-heat measurements

In Fig. 25, we show magnetic specific-heat $C(T)$ data taken over the range of oxygen concentration $0.26 \lesssim x \lesssim 0.93$, from Ref. 28. For $NdBa_2Cu_3O_{6.93}$ we see that there is a sharp specific-heat anomaly near 0.5 K, in agreement with the neutron results.[7] As oxygen is removed we see that the peak in $C(T)$ is rounded, although as more oxygen is removed the peak gets somewhat sharper and occurs at a progressively higher temperature. At $x \simeq 0.3$, the anomaly is again very sharp, and the transition is at the relatively high temperature of $T \simeq 1.75$ K, again in excellent agreement with the neutron results. Hence, both experimental techniques show the same striking oxygen dependence to the magnetic ordering. Lastly, we note that the specific-heat curve in Fig. 25, at high oxygen concentration ($x \gtrsim 0.9$), can be fit by an anisotropic 2D $S = \frac{1}{2}$ Ising model, while at lower concentration the curves are qualitatively described by a 2D Heisenberg system (exhibiting no transition to long-range order), and finally for $x \lesssim 0.3$ the curves are again Ising like.

IX. DISCUSSION OF THE Nd RESULTS

The ordering temperatures for both the fully oxygenated (0.53 K) sample and the deoxygenated sample (1.75 K) are much higher than expected based on dipole interactions alone and a Nd moment $\mu_{Nd} \approx 1\mu_B$. Consider that for a dipole interaction we have $T_N \propto \mu^2$, and for Dy in $DyBa_2Cu_3O_7$, whose ordering temperature (0.93 K) is well estimated from dipole calculations, $\mu_{Dy} \simeq 7\mu_B \approx 7(\mu_{Nd})$, as discussed above.[3] This would imply, from dipole considerations alone, that the ordering temperature for Nd should be at least 50 times lower than that of Dy, yet they both order at temperatures near 1 K. In view of our experimental results, as well as the inability of dipole interactions to yield such high ordering temperatures, there must be an additional magnetic interaction

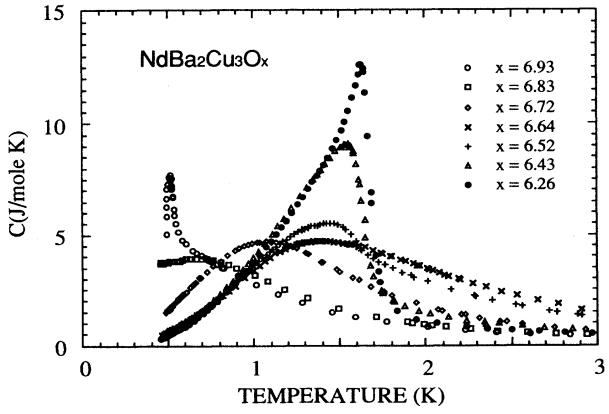

FIG. 25. Magnetic specific heat C vs temperature for the range of oxygen concentration $0.26 \lesssim x \lesssim 0.93$ from Ref. 28.

TABLE II. Oxygen dependence of the rare-earth magnetic order in $R Ba_2Cu_3O_{6+x}$.

Compound	T_c (K)	T_N (K)	$\mu_z(\mu_B)$	$\hat{\mathbf{M}}$	Q	Low T order
$ErBa_2Cu_3O_7$	92	0.62	4.9	b axis	$(\frac{1}{2}\ 0\ \frac{1}{2}),(\frac{1}{2}\ 0\ 0)$	3D long range
$ErBa_2Cu_3O_{6.6}$	75	0.48	3.9 (Ref. 19)	b axis	$(\frac{1}{2}\ 0\ \frac{1}{2}),(\frac{1}{2}\ 0\ 0)$	3D long range
$ErBa_2Cu_3O_6$	0	<0.06		a,b axis	$(\frac{1}{2}\ 0),(0\ \frac{1}{2})$	2D short range
$DyBa_2Cu_3O_7$	90	0.93	7	c axis	$(\frac{1}{2}\ \frac{1}{2}\ \frac{1}{2})$	3D long range
$DyBa_2Cu_3O_{6.54}$	50	0.87	7	c axis	$(\frac{1}{2}\ \frac{1}{2}\ 0)$	3D long range
$DyBa_2Cu_3O_6$	0	0.55 (2D)		c axis	$(\frac{1}{2}\ \frac{1}{2}\ 0)$	2D long range
$NdBa_2Cu_3O_{6.94}$	90	0.53	1.1 (Ref. 7)	c axis	$(\frac{1}{2}\ \frac{1}{2}\ \frac{1}{2})$	3D long range
$NdBa_2Cu_3O_{6.78}$	63				$(\frac{1}{2}\ \frac{1}{2})$	2D short range
$NdBa_2Cu_3O_{6.45}$	0				$(\frac{1}{2}\ \frac{1}{2}\ \frac{1}{2})$	3D short range
$NdBa_2Cu_3O_{6.3}$	0	1.5		45° off c axis	$(\frac{1}{2}\ \frac{1}{2}\ \frac{1}{2})$	3D long range
$NdBa_2Cu_3O_{6.13}$	0	1.75	0.85	45° off c axis	$(\frac{1}{2}\ \frac{1}{2}\ \frac{1}{2})$	3D long range

between rare-earth ions, and this interaction must involve the chain layer oxygen ions since T_N varies drastically with x. The specific-heat results on $NdBa_2Cu_3O_{6.93}$ can also be better understood in terms of such a coupling. The $NdBa_2Cu_3O_{6.93}$ data in Fig. 25 fit very nicely to an anisotropic 2D $S=\frac{1}{2}$ Ising model, and a strong coupling of the Nd spins via the chain layer could be the origin of this anisotropy.

Inelastic neutron-scattering measurements indicate that the crystal-field magnetic ground state of Nd is effectively unchanged over the whole range of oxygen concentration, $0 \leq x \leq 1$.[31] However, single-ion crystal-field calculations do reveal that the easy magnetic axis goes from the c axis in fully oxygenated $NdBa_2Cu_3O_7$ to isotropic behavior close to $x \simeq 0.8$, and by further reducing the oxygen concentration the a axis becomes the easy magnetic axis.[31] The change in the easy axis of magnetization may explain why we see a change in the moment direction from parallel to c ($\mu \| c$) in $NdBa_2Cu_3O_7$, to $\approx 45°$ off the c axis for our deoxygenated insulating samples with $x \leq 0.3$. Also, if the moment direction is truly isotropic near $x \simeq 0.8$, then a 2D Heisenberg model would be appropriate and this would explain the loss of long-range order. Recent work by Allenspach, Maple, and Furrer[4] lends support to the Nd spins being 2D Heisenberg-like near $x \simeq 0.8$, as they have had reasonable success fitting the magnetic specific-heat data at $x \simeq 0.72$ with a 2D $S=\frac{1}{2}$ Heisenberg cluster model. More quantitative work is needed to determine if, indeed, this is a mechanism for any of the oxygen dependence of the Nd ordering we see.

A summary of our results on the oxygen dependence of the rare-earth magnetic order is given in Table II. We have found that all three rare-earth magnetic systems are very sensitive to the chain layer oxygen concentration. This is somewhat surprising considering the generally accepted view that the rare-earth ions are electronically isolated from the superconducting Cu-O planes.[1] Even more remarkable is the fact that the rare-earth magnetism of all of the materials we studied has a different oxygen dependence. $ErBa_2Cu_3O_7$ displays 3D long-range order, and as oxygen is removed T_N decreases until in nominally oxygenated insulating $ErBa_2Cu_3O_{6+x}$ ($x \approx 0$) only 2D short magnetic correlations are observed. In $DyBa_2Cu_3O_{6+x}$ T_N also decreases with oxygen, but the spin structure changes with oxygen content as well, going from antiparallel along the c axis ($x \simeq 1$), to parallel while still in the superconducting phase ($x < 1$). In $NdBa_2Cu_3O_{6+x}$ T_N *increases* threefold as oxygen is reduced from $x \simeq 1$ ($T_N = 0.53$ K) to $x \lesssim 0.3$ ($T_N \simeq 1.5$ K), while only short-range order is observed for $0.3 < x < 1$. Also, while T_N for $ErBa_2Cu_3O_{6+x}$ and $DyBa_2Cu_3O_{6+x}$ is fairly well estimated by dipole interactions, in $NdBa_2Cu_3O_{6+x}$ T_N is at least 50 times larger than dipole estimates. These results demonstrate unambiguously that dipole interactions are incapable of explaining the variety of magnetic structures and Néel temperatures observed, and that there is a significant coupling between the chain layer oxygen and the rare-earth magnetism. More studies will be required to fully elucidate the nature of this coupling.

ACKNOWLEDGMENTS

We would like to thank S. Skanthakumar and N. Bartelt for many helpful conversations. We thank Qing-Zhen Huang for helping us with the profile refinements, and T. Vanderhah and M. Osofsky for making available a Dy123 crystal to confirm the behavior observed throughout these studies. One of the authors (M.B.) acknowledges partial support by the Alexander von Humboldt-Stiftung. Research at Maryland is supported by the NSF, DMR 93-02380. Research at U.C. Davis is supported by the NSF, DMR 94-03895. Research at UCSD was supported by the U.S. Department of Energy, Grant No. DE-FG03-86ER45230.

[1]A recent review of the oxide superconductors is given in *High Temperature Superconductivity,* edited by J. W. Lynn (Springer-Verlag, New York, 1990).

[2]Y. Nakazawa, M. Ishikawa, and T. Takabatake, Physica B **148**, 404 (1987); S. Simizu, G. H. Bellesis, J. L. Lukin, S. A. Friedberg, H. S. Lessure, S. M. Fine, and M. Greenblatt, Phys. Rev. B **39**, 9099 (1989).

[3]T. W. Clinton, Ph.D. thesis, University of Maryland, 1992.

[4]P. Allenspach, M. B. Maple, and A. Furrer, J. Alloys Comp. (to be published).

[5]K. N. Yang, J. M. Ferreira, B. W. Lee, M. B. Maple, W.-H. Li, J. W. Lynn, and R. W. Erwin, Phys. Rev. B **40**, 10 963 (1989); T. W. Clinton, J. W. Lynn, B. W. Lee, M. Buchgeister, and M. B. Maple, J. Appl. Phys. **73**, 6321 (1993).

[6]J. W. Lynn, T. W. Clinton, W.-H. Li, R. W. Erwin, J. Z. Liu, K. Vandervoort, and R. N. Shelton, Phys. Rev. Lett. **63**, 2606 (1989); J. W. Lynn, T. W. Clinton, W.-H. Li, R. W. Erwin, J. Z. Liu, R. N. Shelton, and P. Klavins, J. Appl. Phys. **67** (9), 4533 (1990); T. W. Clinton, J. W. Lynn, J. Z. Liu, Y. X. Jia, and R. N. Shelton, J. Magn. Magn. Mater. **104-107**, 625 (1992); Physica C **217**, 53 (1993); T. W. Clinton, Ph.D. thesis, University of Maryland, 1992.

[7]K. N. Yang, J. M. Ferreira, B. W. Lee, M. B. Maple, W.-H. Li, J. W. Lynn, and R. W. Erwin, Phys. Rev. B **40**, 10 963 (1989). For additional neutron-scattering work on $NdBa_2Cu_3O_7$ see P. Fischer, B. Schmid, P. Brüesch, F. Stucki, and P. Unternährer, Z. Phys. B **74**, 183 (1989).

[8]T. W. Clinton, J. W. Lynn, B. W. Lee, M. Buchgeister, and M. B. Maple, J. Appl. Phys. **73**, 6320 (1993).

[9]D. L. Kaiser, F. Holtzberg, B. A. Scott, and T. R. Mcguire, Appl. Phys. Lett. **51**, 1050 (1987).

[10]T. W. Clinton, J. W. Lynn, J. Z. Liu, Y. X. Jia, and R. N. Shelton, J. Appl. Phys. **70**, 5751 (1991).

[11]H. Shaked, B. W. Veal, J. Faber, Jr., R. L. Hittermann, U. Balachandran, G. Tomlins, H. Shi, L. Morss, and A. P. Paulikas, Phys. Rev. B **41**, 4173 (1990).

[12]L. Onsager, Phys. Rev. **65**, 117 (1944).

[13]C. N. Yang, Phys. Rev. **85**, 808 (1952).

[14]T. Chattopadhyay, P. J. Brown, D. Bonnenberg, S. Ewert, and H. Malleta, Europhys. Lett. **6**, 363 (1988); T. Chattopadhyay, P. J. Brown, B. C. Sales, L. A. Boatner, H. A. Mook, and H. Maletta, Phys. Rev. B **40**, 2624 (1989).

[15]D. McK. Paul, H. A. Mook, L. A. Boatner, B. C. Sales, J. O. Ramey, and L. Cussen, Phys. Rev. B **39**, 4291 (1989).

[16]T. W. Clinton, J. W. Lynn, J. Z. Liu, Y. X. Jia, and R. N. Shelton, Physica C **217**, 53 (1993).

[17]R. J. Birgeneau, H. J. Guggenheim, and G. Shirane, Phys. Rev. B **1**, 2211 (1970).

[18]Huai Zhang, J. W. Lynn, W.-H. Li, T. W. Clinton, and D. E. Morris, Phys. Rev. B **41**, 11 229 (1990); Huai Zhang, J. W. Lynn, and D. E. Morris, *ibid.* **45**, 10 022 (1992).

[19]H. Maletta, E. Pörschke, T. Chattopadhyay, and P. J. Brown, Physica C **166**, 9 (1990).

[20]K. De'Bell and J. P. Whitehead, J. Phys. Condens. Matter **3**, 2431 (1991); A. B. MacIsaac, J. P. Whitehead, K. De'Bell, and K. Sowmya Narayanan (unpublished).

[21]S. K. Misra and J. Felsteiner, Phys. Rev. B **46**, 11 033 (1992).

[22]For more details on a spin system with a fourfold degenerate ground state see J. V. José, S. Kirkpatrick, L. P. Kadanoff, and D. R. Nelson, Phys. Rev. B **16**, 1217 (1977); L. D. Roelofs and P. J. Estrup, Surf. Sci. **125**, 51 (1983); A. Sadiq and K. Binder, J. Stat. Phys. **35**, 517 (1984).

[23]A. I. Buzdin and L. N. Bulaevskii, JETP Lett. **47**, 327 (1988).

[24]S. H. Liu, Phys. Rev. B **37**, 7470 (1988).

[25]J. A. Hodges, P. Bonville, P. Imbert, and G. Jéhanno, Physica C **184**, 283 (1991); **184**, 259 (1991).

[26]A. I. Goldman, B. X. Yang, J. Tranquada, J. E. Crow, and C.-S. Jee, Phys. Rev. B **36**, 7234 (1987).

[27]P. Fischer, K. Kakurai, M. Steiner, K. N. Clausen, B. Lebechi, F. Hulliger, H. R. Ott, P. Brüesch, and P. Unternahrer, Physica C **152**, 145 (1988).

[28]B. W. Lee, J. M. Ferreira, S. Ghamaty, K. N. Yang, and M. B. Maple, in *Oxygen Disorder Effects in High T_c Superconductors,* edited by J. L. Moran-Lopez and I. K. Schuller (Plenum, New York, 1990), p. 151.

[29]B. E. Warren, Phys. Rev. **59**, 693 (1941).

[30]For a discussion of magnetic scattering measurements made on single-crystal vs powder samples see T. W. Clinton and J. W. Lynn, Physica C **174**, 487 (1991); T. W. Clinton, J. W. Lynn, J. Z. Liu, Y. X. Jia, and R. N. Shelton, *ibid.* **217**, 53 (1993).

[31]P. Allenspach, J. Mesot, M. Guillaume, and A. Furrer (unpublished); see also P. Allenspach, B. W. Lee, D. Gajewski, and M. B. Maple (unpublished).